ELSEVIER

Journal of Structural Geology xx (xxxx) 1–24

JOURNAL OF STRUCTURAL GEOLOGY

www.elsevier.com/locate/jsg

The quantitative link between fold geometry, mineral fabric and mechanical anisotropy: as exemplified by the deformation of amphibolites across a regional metamorphic gradient

Lenka Baratoux[a,*], Ondrej Lexa[a,b], John W. Cosgrove[c], Karel Schulmann[b]

[a]*Institute of Petrology and Structural Geology, Charles University, Albertov 6, Praha 2, 12843, Czech Republic*
[b]*Université Louis Pasteur, EOST, UMR 7517, 1 Rue Blessig, Strasbourg 67084, France*
[c]*Department of Earth Science & Engineering, Royal School of Mines, Imperial College of Science, Technology & Medicine, Prince Consort Road, London SW7 2BP, UK*

Received 8 June 2004

Abstract

This work shows lateral variations in fold geometry within an amphibolite unit of constant mineralogical composition under increasing metamorphic grade. Analysis of the fold geometries indicate: (1) medium amplification associated with low post-buckle flattening in the garnet zone, (2) high amplification coupled with medium post-buckle flattening in the staurolite zone, and (3) passive amplification dominated by intense post-buckle flattening in the sillimanite zone. A systematic decrease in the mechanical anisotropy of the folded fabric is observed with increase in metamorphic grade. Quantitative microstructural study shows contrasting deformation micro-mechanisms associated with folding manifested by: (1) brittle dominated deformation of amphiboles that form a stress supporting network with a high competence contrast with respect to plagioclase in the garnet zone, (2) ductile dominated heterogeneous deformation of an interconnected weak layer structure with low competence contrast in the staurolite zone, and (3) homogeneous deformation of a stress supporting framework with low competence contrast in the sillimanite zone. The difference in the folding style between the garnet and staurolite zones is associated with the lateral variations in microstructure of the amphibolites inherited from a pre-folding metamorphic zonation and with different deformation mechanisms in the hinge zones. However, the change in fold style observed as one moves into the sillimanite zone is controlled by the recrystallization associated with an important syn-folding heat input from an adjacent granite intrusion.

Keywords: Fold geometry; Quantitative link; Amphibolite; Metamorphic gradient; Deformation microstructures

1. Introduction

The fold shape in a folded bilaminate is determined by the ratio of competent to incompetent layer thickness and the viscosity contrast (μ_1/μ_2) between them (Ramberg, 1961). Ramsay and Huber (1987, p. 405) discuss the factors that influence the fold geometry of such buckled bilaminates. The most important factors are the primary rheological properties of the layers, which depend on the mineralogical composition and grain size, external parameters such as temperature and pressure, and the development of a preferred orientation of minerals during deformation. The seminal work of Biot (1961) provided a theoretical treatment capable of analysing these systems and his work has been successfully applied by geologists to explain the buckling behaviour of both discretely layered systems and mineral fabrics. In Biot's work the most important factor controlling the mode and style of folding is the mechanical anisotropy of the material. It can be shown that there is a direct link between the mechanical anisotropy and the competence contrast of a bilaminate (μ_1/μ_2) and this allows one to use both theories to study their folding behaviour (Price and Cosgrove, 1990). By analysing the geometries of the studied folds it is possible to determine which of the two theoretical approaches is more appropriate.

Although a large quantity of work has been carried out on the folding mechanics of layered systems (e.g. the theoretical work by Biot (1961, 1963a,b), Ramberg (1963,

* Corresponding author. Tel.: +420-257189509
E-mail address: lka@natur.cuni.cz (L. Baratoux).

0191-8141/$ - see front matter © 2005 Elsevier Ltd. All rights reserved.
doi:10.1016/j.jsg.2005.01.001

1964) and Fletcher (1995), the experimental studies by Ghosh (1968), Dubey and Cobbold (1977), Dubey (1980), Mancktelow and Abbassi (1992) and Hobbs (1971) and the field studies by Oertel and Ernst (1978) and Fowler and Winsor (1996)), this work is not directly applicable to the folding of mineral fabrics where the concept of layer thickness and competence contrast are more difficult to define. Fortunately a theory of the deformation of mechanically anisotropic materials has been developed by Biot (1967), which enables the folding of mineral fabrics to be considered.

The application of modern computer graphics, in particular geographic information systems (GIS) in quantitative petrography, and computer techniques, which allow the precise evaluation of grain shapes (Panozzo, 1983, 1984), grain sizes and grain spatial distribution, have provided tools for the assessment of the relationship between mineral fabrics and the folding that develops within them. In this paper we present a method of quantitative microstructural analysis that allows the semi-quantitative assessment of the mechanical anisotropy of mineral fabrics. We demonstrate that quantitative computer-aided analysis of natural fold shapes in conjunction with a study of the internal microstructure allows a better understanding of the mechanical behaviour of naturally folded multilayers. Our observations show that it is possible to distinguish folds formed by active buckling from those dominantly controlled by passive amplification. This can be clearly correlated with major variations in mineral microstructures, semi-quantitatively estimated mechanical anisotropy and the deformation mechanisms associated with folding.

The rock unit studied in this analysis consists of metabasites of relatively constant composition that show metamorphic zonality ranging from the lower amphibolite facies conditions in the east to the upper amphibolite facies conditions in the west. The metamorphism was accompanied by the development of progressively evolving mineral microfabrics forming a gently dipping to sub-horizontal metamorphic foliation. This consistently oriented but systematically varying rock anisotropy has been subsequently affected by horizontal compression responsible for the development of upright post-metamorphic folds. In addition, a granite intruded into the western part of the amphibolite sheet and thermally influenced the host rock within a zone several kilometres wide. Field observations show a remarkable change in the style of the post-peak metamorphic folding approaching the intrusion (Schulmann and Gayer, 2000) and the question arises as to whether the change in fold style reflects the variation in the inherited mechanical anisotropy associated with the east–west metamorphic–microfabric zonation, whether it is related to the lateral heat input from the westerly granite, or both.

The aims of this contribution are: (1) the quantitative characterization of the fold shapes and semi-quantitative determination of mechanical anisotropy based on quantitative microstructural analysis, (2) the determination of possible folding mechanisms using fold shape analysis as well as the micro-deformational mechanisms associated with folding, and (3) the evaluation of the relative role of the inherited paleometamorphic microstructural zonation (mechanical anisotropy) and lateral heating, on folding.

2. Geological setting

The northeastern margin of the Bohemian massif is built up of the Neo-Proterozoic basement called Brunia and its sedimentary cover (Dudek, 1980) in the east, and a belt of Brunia derived Variscan nappes (Silesian domain) with high grade rocks of the orogenic root belonging to the Lugian domain in the west (Fig. 1).

The studied area is located in the Brunia derived par-autochthon called the Desná dome, which consists of metamorphic Neo-Proterozoic basement core surrounded by a volcano-sedimentary Devonian envelope (Fig. 1b). Metabasites of the Jeseník amphibolite massif, the subject of this study, form part of this Devonian sequence. The huge accumulation of basic rocks was formed during the Early Devonian rifting, as indicated by their tectono-stratigraphic position and back-arc tholeiitic composition (Patočka and Valenta, 1990). Metabasites are present on both the eastern and western flanks of the Desná gneissic core. The basites at the eastern margin show more tuffitic character while the main amphibolite body situated in the west developed mostly from basalts and possibly from gabbros as indicated by preserved textures in the less deformed domains. The metabasites are locally stratigraphically or tectonically intercalated with metapelites and quartzites of Pragian age (Chlupáč, 1994), which show the same tectono-metamorphic history.

2.1. Structural geology

The complex polyphase tectonic evolution of the region comprises the early pre-Variscan deformations termed D_1. The first Variscan structures are associated with the Barrovian metamorphism (termed D_2), and the late Variscan structures (D_3), developed during the transpressional regime. The most important D_2 structure is represented by a planar metamorphic fabric expressed as localized shear zones in the basement orthogneisses and as a penetrative, originally sub-horizontal metamorphic foliation (S_2) in all the rocks of the Devonian cover. This fabric is now dipping to the NW or SE at moderate to steep angles as a result of subsequent large-scale folding (Fig. 2a). Within the cover, syn-schistose folds (F_2) as well as mineral lineation (L_2) are locally well developed.

The D_3 deformation had various effects on different lithologies, depending mainly on the intensity of the previous S_2 anisotropy (Schulmann and Gayer, 2000).

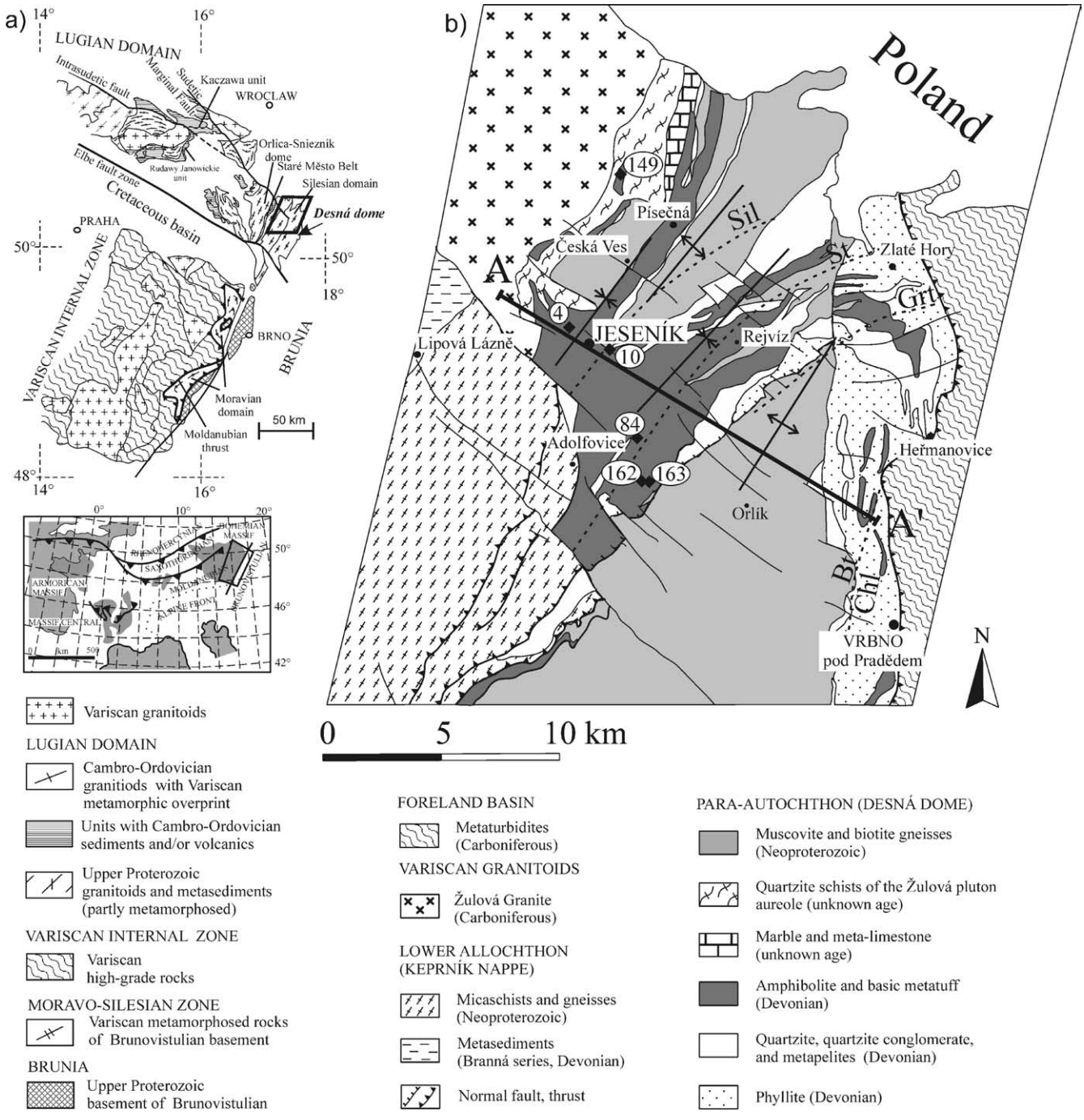

Fig. 1. (a) Geological map of the eastern margin of the Bohemian Massif. Inset shows location of the studied area in the frame of European Variscides. (b). Geological map of the Silesian domain based on the geological map 1:200,000 by Pouba (1962) and Roth (1962). Important thrust faults and normal faults are indicated. A–A′ indicates the position of the cross-section in Fig. 2.

Basement orthogneisses display rare upright folding. Metabasites and metasediments of the Devonian volcano-sedimentary cover show well-developed mostly asymmetric F_3 folds with axial planes dipping to the NW or SE and subhorizontal NE–SW-trending hinges (Fig. 2a). The fold size ranges from the microscopic grain-scale up to metres-scale folds. In the eastern and central parts of the Desná dome the D_3 deformation was post-peak metamorphic and took place under greenschist conditions as marked by growth of chlorite, muscovite and albite along axial cleavage of F_3 folds in metapelites (Schulmann and Gayer, 2000). However, it was contemporaneous with the emplacement of the Žulová granite in the west (Cháb and Žáček, 1994; Schulmann and Gayer, 2000), which resulted in the overprinting of the S_2 foliation by a NE–SW-trending steep and penetrative foliation S_{2-3} (Fig. 2a).

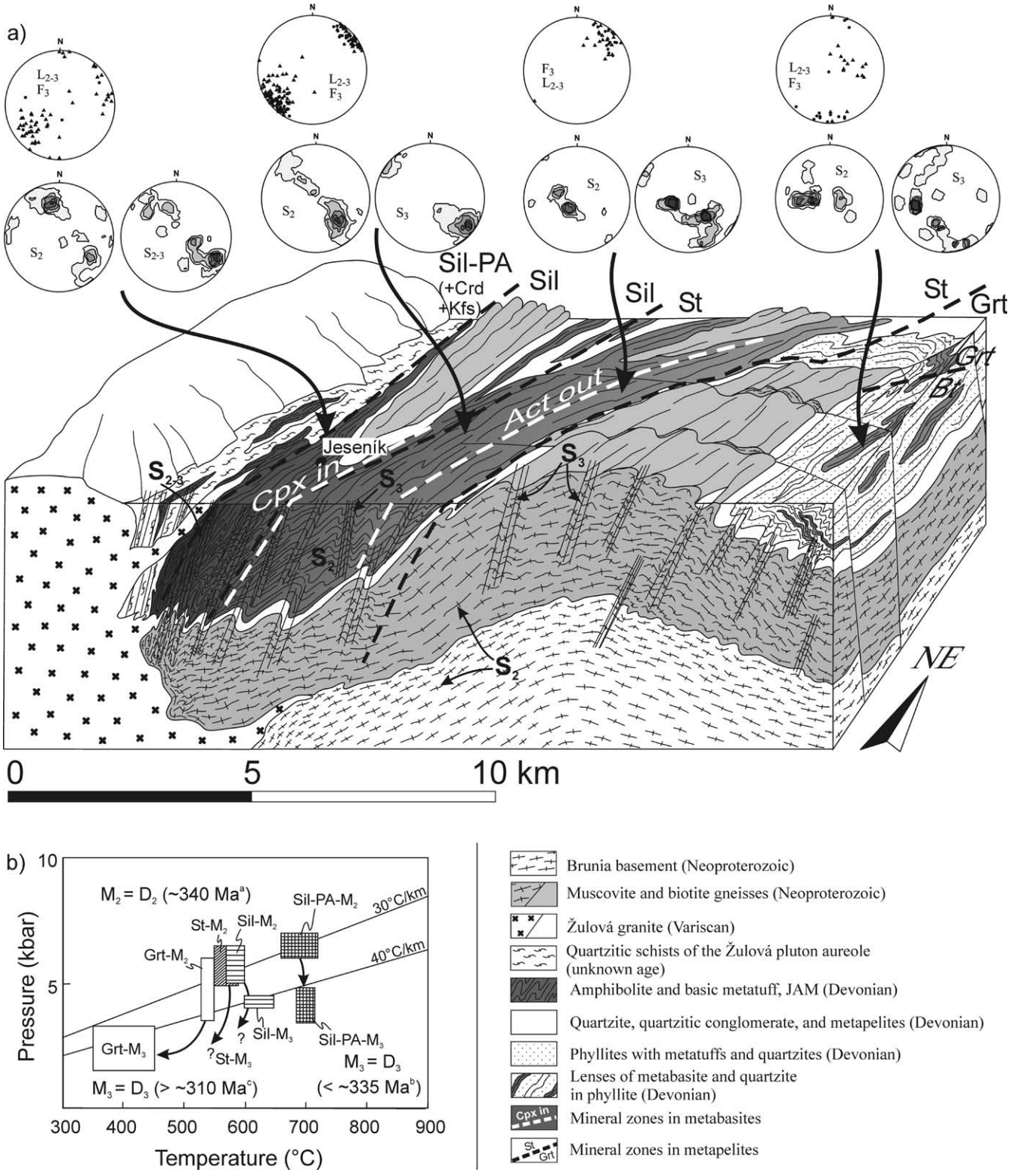

Fig. 2. Geological cross-section A–A′ (shown in Fig. 1b) of the Desná dome showing major structures, lithology of individual units, and major tectonic boundaries (a). Metamorphic zones extended from metapelites are indicated as well as approximate actinolite-out and clinopyroxene-in isograds (for Ca-rich metabasites). Equal area lower hemisphere stereoplots are shown for D_2, and D_3 planar and linear structures. Each stereoplot contains between 50 and 100 poles contoured as multiples of uniform distribution. The cross-section is constructed from photographs and field notes and shows the principal structural features. The vertical axis is not to scale. Note that the metamorphic isograds cross-cut lithological boundaries and their apparent steep attitude is associated with a large scale F_3 folding of their original flat dip as shown by Schulmann and Gayer (2000) and Štípská et al. (2000). (b) Lower left inset shows PT plot with indicated ages of M_3 and M_2 metamorphisms and associated fabrics; a—Schulmann and Gayer (2000); b—Jehlička (1995); c—Maluski et al. (1995). PA — pluton aureole.

2.2. Metamorphic zonality

The Variscan metamorphic evolution of the study area involves two main phases; an M_2 metamorphism of Barrovian character with the intensity increasing westwards and an M_3 metamorphism induced by the Žulová granite intrusion in the western margin of the Desná dome. The Barrovian M_2 metamorphic grade ranges from chlorite zone in the eastern margin of the Desná dome up to staurolite and possibly sillimanite zone in the west. The M_3 periplutonic HT/LP overprint also attains its maximum in the western part of the studied area, where it is documented by the presence of K-feldspar–cordierite migmatites (Rozkošný and Souček, 1989; Cháb and Žáček, 1994), as well as by the growth of sillimanite and new garnet in the staurolite micaschists in the pluton aureole (Fig. 2).

Although the metabasites cannot be precisely divided into particular metamorphic zones once they have reached amphibolite facies conditions, it is nevertheless necessary for the purpose of this work to establish a metamorphic zoning of the amphibolite massif based on the increasing metamorphic conditions. The metamorphic zones determined in intercalated metasedimentary rocks by Souček (1978) are therefore extended into the adjacent metabasites and used as a reference for the definition of the metamorphic grade therein. The justification for this procedure is based on the mutual field relations of the amphibolites and metasediments, which indicate that both lithologies have experienced the same tectonic and metamorphic history (Schulmann and Gayer, 2000). Therefore, PT conditions were determined in metasediments applying various thermobarometry methods (Baratoux, 2004). The degree of metamorphism in the east of the metabasite massif corresponds to the garnet zone in the contiguous metasediments and the mineral assemblage in the metabasites includes hornblende, plagioclase, actinolite, chlorite, and epidote corresponding to PT conditions of 540 ± 10 °C and 5 ± 1 kbar. Further to the west actinolite and epidote disappear and $Hbl + Pl \pm Qtz + Ilm + Ttn$, which corresponds to the staurolite zone, appears with metamorphic conditions of M_2 estimated to be 570 ± 30 °C and 5.5 ± 1 kbar (Baratoux, 2004). The mineral assemblage in the metabasites corresponding to the sillimanite zone is represented by $Hbl + Pl \pm Qtz + Ilm + Ttn$ and $Amp + Pl \pm Qtz \pm Cpx \pm Cal + Ilm + Ttn$ in calcium-rich lithologies and metamorphic conditions of this zone were estimated to 590 ± 20 °C and 5.5 ± 1 kbar. In the pluton aureole, sillimanite–cordierite–K-feldspar assemblage occur in metapelites and the PT conditions of periplutonic M_3 metamorphism reached 700 ± 15 °C and 4.2 ± 0.8 kbar (Fig. 2b). The mineral assemblage in the amphibolites corresponds to that of the sillimanite zone.

The age of the main fabric-forming M_2 metamorphic event is difficult to establish in the studied area, but it is supposed to have occurred during the main collisional event, which is dated elsewhere at ~340 Ma (Schulmann and Gayer, 2000; Štípská et al., 2004). The termination of the D_2–M_2 event can be constrained by Rb–Sr dating (335 ± 7.5 Ma) of the crystallization of the Žulová granite (Jehlička, 1995). However, $^{40}Ar/^{39}Ar$ dating of muscovite and biotite from mylonitic gneisses of the Desná dome and of the Žulová granite (Maluski et al., 1995) suggest that cooling through the white mica and biotite closure temperatures (350 and 300 °C, respectively) occurred between 310 and 300 Ma. Therefore, this age may correspond to the greenschist facies F_3 folding activity in the east and to the cooling of the Žulová pluton to the west.

3. D_2 and D_3 amphibolite microstructures across metamorphic zones

3.1. Eastern part of the massif (the garnet zone)

In the eastern part of the massif, i.e. in the garnet zone, some weakly deformed metagabbros with large grains of hornblende and plagioclase (1–2 mm) are still present. The main metamorphic fabric S_2 of amphibolites is preserved in domains unaffected by F_3 folding or in F_3 fold limbs and it is characterized by a strong mineral shape preferred orientation (SPO) of amphibole 0.2–3 mm in size (Fig. 3a). These grains often show a strong chemical zonality with actinolitic cores and tschermakitic rims (Fig. 4a). Fine-grained (30–60 μm) sub-equant plagioclase ($An_{25–35}$) forms elongate polycrystalline aggregates surrounded by laths of amphibole. These new grains develop from large relict clasts ($An_{40–50}$) (Fig. 4d). The plagioclase in these domains exhibits features typical for dynamic recrystallization (in the sense of Poirier and Guillopé (1979)) such as undulatory extinction, the development of sub-grain boundaries, and a uniform grain-size distribution. However, a contribution of metamorphic nucleation is evidenced by the different chemical composition of the host and the new grains (Rosenberg and Stünitz, 2003).

In the hinge zones of F_3 microfolds, amphibole grains with irregular boundaries are commonly bent and broken (Fig. 3b). Microfractures associated with domainal undulatory extinction fragment large grains into smaller elongate segments. There is no difference in plagioclase microstructure in the non-folded foliation and in the crenulated domains. It is concluded, therefore, that the main D_3 deformation mechanism for amphibole is fracturing (in the sense of Nyman et al. (1992) and Stünitz (1993)) and passive grain rotation within the plagioclase matrix.

3.2. Central part of the massif (the staurolite zone)

In the eastern part of the central zone of the massif actinolite is still locally present in the cores of dark green grains of magnesio-hornblende. Amphibole composition follows the pargasitic line (Fig. 4b) within the S_2 foliation. The size of the dark green grains of magnesio-hornblende

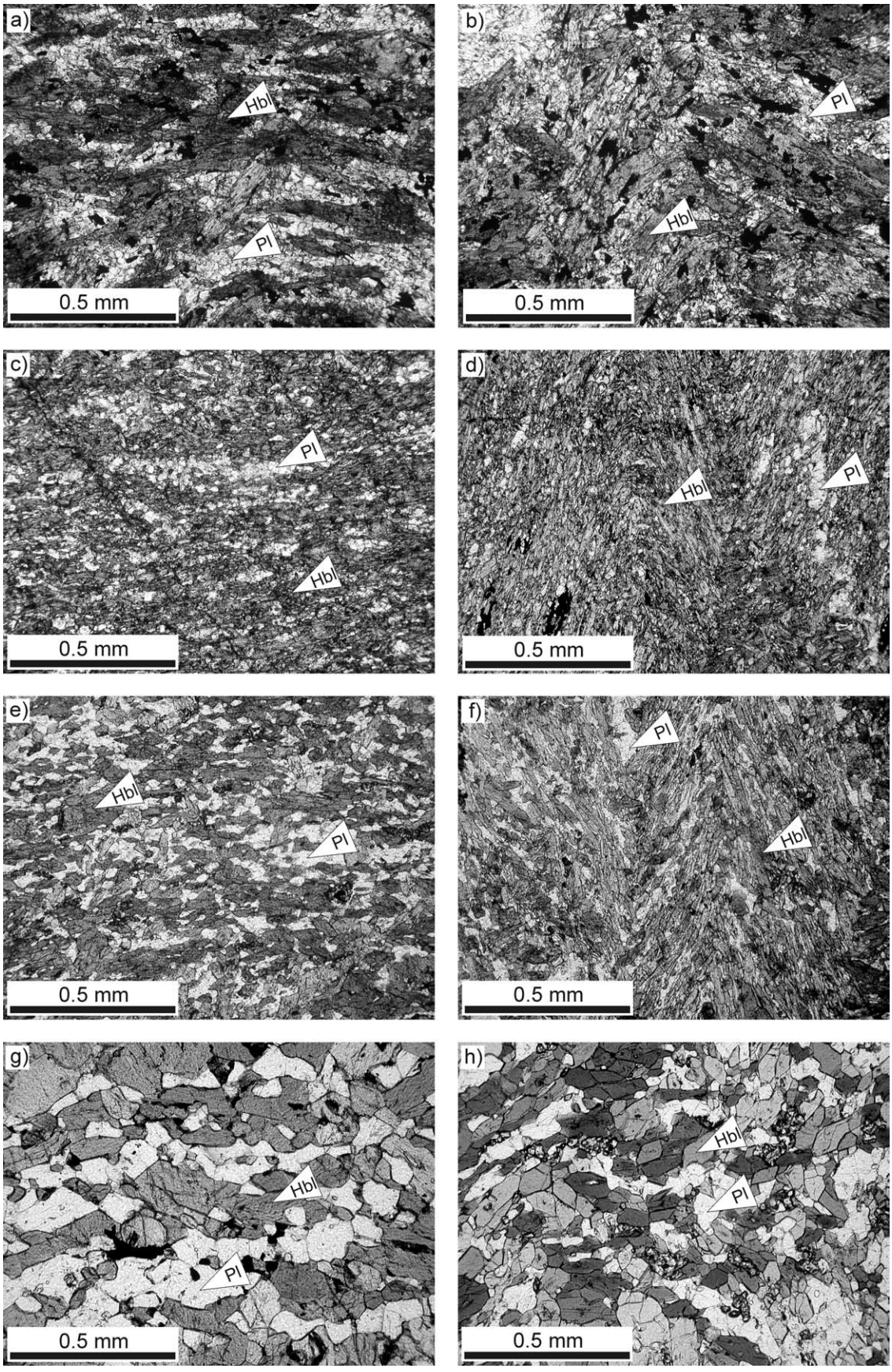
a)
Hbl
Pl
0.5 mm
b)
Pl
Hbl
0.5 mm
c)
Pl
Hbl
0.5 mm
d)
Hbl
Pl
0.5 mm
e)
Hbl
Pl
0.5 mm
f)
Pl
Hbl
0.5 mm
g)
Hbl
Pl
0.5 mm
h)
Hbl
Pl
0.5 mm

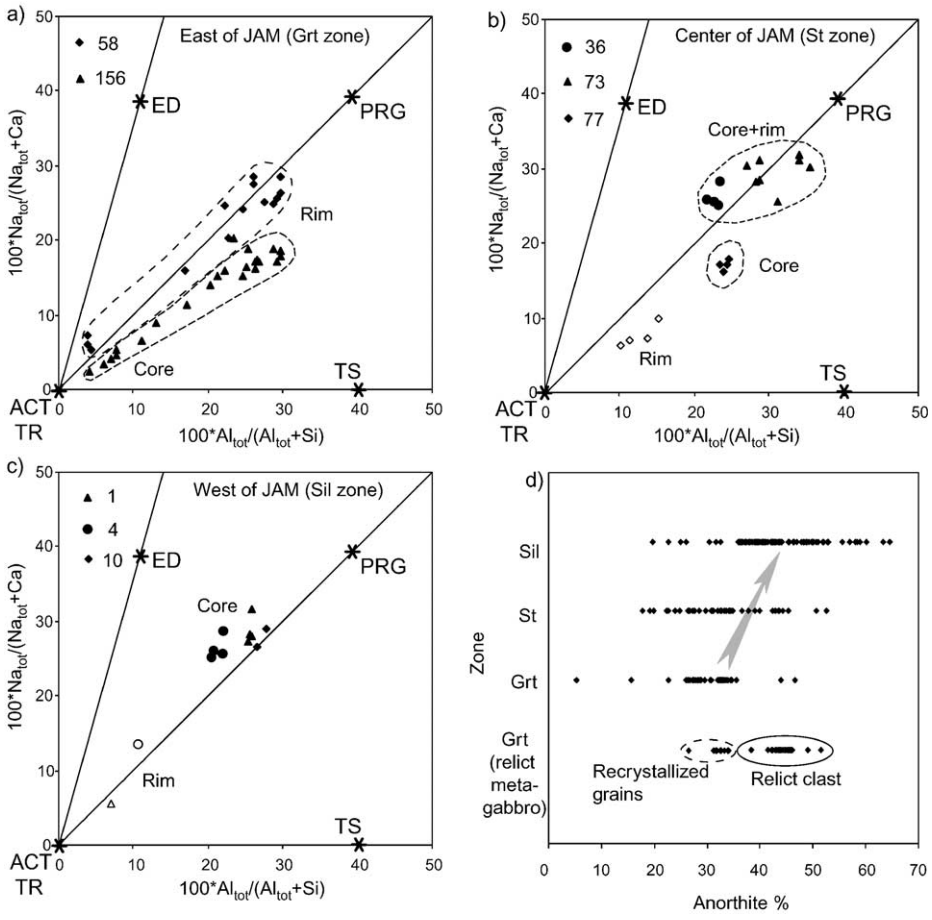

Fig. 4. The evolution of amphibole (a)–(c) and plagioclase (d) compositions in the garnet, staurolite and sillimanite zones. In (a)–(c) the compositions situated below the pargasitic line (PRG) in the garnet and straurolite zones are interpreted as relics of previous metamorphic or magmatic stage while those following or situated above the pargasitic line are thought to be of metamorphic origin (for further discussion see Baratoux (2004)). The numbers next to the symbols correspond to the analysed samples. Sample 1 in the sillimanite zone is situated in the pluton aureole. Compositions of end members edenite (ED), pargasite (PRG), tschermakite (TS), actinolite (AC), and tremolite (TR) are indicated.

varies from fine-grained (0.01–0.1 mm), through medium-grained (0.1–1 mm), up to coarse-grained (0.5–3 mm) porphyroblasts. The finer the amphibole grains, the stronger their SPO and alignment are. The sub-equant, weakly elongate plagioclase of $An_{25–35}$ composition and 20–50 μm in size is either randomly distributed among the amphiboles or forms either elongate polycrystalline aggregates or layers alternating with the amphibole planar fabric (Fig. 3c). Straight boundaries of sub-equant plagioclase grains commonly meet in triple junctions.

In the hinge zones of F_3 folds, large amphiboles are generally bent and fractured (Fig. 3d). The main difference with respect to the previous zone is an important grain size reduction of amphibole down to 0.01–0.05 mm as a result of fracturing. New grains attain lower aspect ratios and become mixed with plagioclase of the same grain size. There is no difference in chemical composition of either the plagioclase or amphibole in the hinge zones compared with the unfolded S_2 fabric.

3.3. Western area of the massif (the sillimanite zone)

In the western area of the massif, i.e. in the sillimanite zone, there is a major change in the microstructural

Fig. 3. Photomicrographs of representative microstructures for each zone. (a) Large amphibole grains parallel to the S_2 foliation in the garnet zone are surrounded by fine-grained recrystallized plagioclase. (b) In the hinge area, amphiboles included within a sub-equant plagioclase matrix grains are bent and broken as a result of micro-folding. (c) Amphibole and plagioclase in the limb area of the staurolite zone tend to form alternating aggregates elongated parallel to the foliation. (d) Microcrenulation leads to strong grain size reduction via brittle deformation of amphibole resulting in the mixing of amphibole and plagioclase in the hinge areas. (e) Plagioclase and amphibole in the sillimanite zone show straight equilibrated boundaries. Both minerals are arranged parallel to the S_2 foliation. (f) Amphibole and plagioclase grains of the hinge area deformed by microcrenulation achieve a high aspect ratio. They reorient sub-parallel to the axial plane without any internal deformation. (g) Foam-like texture with straight equilibrated grain boundaries meeting at triple junctions of 120° as well as a high grain size in both minerals is typical of the metabasites of the pluton aureole. Amphibole and plagioclase tend to form separate monomineral layers. (h) Amphibole and plagioclase texture in the hinge zone of microfolds is similar to that in the limbs.

character of the metabasites compared with those in the garnet and staurolite zones. Brownish green ferroan pargasitic grains of hornblende with aspect ratios of 2–4 are arranged parallel to the S_2 fabric (Fig. 4c). They display mutual equilibrated straight grain boundaries typical of high-grade amphibolite textures (Brodie and Rutter, 1985). Unlike the staurolite zone where the plagioclase ($An_{30–60}$) tends to form layers, we observe isolated grains and aggregates of plagioclase surrounded by elongate and well oriented crystals of amphibole (Fig. 3e). Chemical zonality and a large span of plagioclase compositions evolving towards anorthite document prograde metamorphic growth associated with dynamic recrystallization (Yund and Tullis, 1991) (Fig. 4d).

The hinge zones of micro-crenulations are very narrow and the amphibole grains tend to reorient parallel with the fold axial planes without any bending and fracturing (Fig. 3f). The hornblende grains show straight boundaries, local decussate structures, and a similar aspect ratio and size to those within limb zones. Plagioclase reaches slightly higher aspect ratios and grain size compared with the limbs. All these features together with the absence of any compositional zoning of the pargasitic hornblende (Fig. 4c) indicate grain growth related to prograde metamorphism (Vernon, 1976).

3.4. Western area of the massif (the sillimanite zone of the pluton aureole)

Unlike the zones described above, brown pargasitic hornblende rich in Ti within the sillimanite zone of the pluton aureole, exhibits straight or slightly concave equilibrated boundaries and fairly low aspect ratios (1.5–2). It is difficult if not impossible to distinguish in thin section the S_2 and S_3 fabrics. In most of the studied samples the pargasitic hornblende is associated with plagioclase ($An_{30–60}$) of similar aspect ratios and size and arranged into a regular 'static' foam-like structure (Fig. 3g). The latter exhibits straight growth-related twins. Plagioclase-rich and amphibole-rich compositional bands are locally developed. Both minerals attain the same size ranging between 0.05 and 0.5 mm. 120° triple point junctions are formed by amphibole–amphibole, plagioclase–plagioclase, and even amphibole–plagioclase grain boundaries. All of the features described above are consistent with re-equilibration under high temperature conditions corresponding to the M_3 HT/LP metamorphic overprint. The hinges of F_3 microfolds are extremely rare but if present they show very similar microstructural relations of hornblende and plagioclase to that of the main fabric (Fig. 3h). A characteristic feature is the growth of large elongate hornblende crystals parallel to the axial plane of the F_3 microfolds. The texture of these rocks bears a remarkable resemblance to the upper amphibolite to granulite facies example of Brodie and Rutter (1985, p. 155).

4. Fold shape analysis

4.1. Methods of quantitative analysis

For the purpose of the fold analysis, 3–6 photographs of representative fold types from each metamorphic zone (garnet, staurolite and sillimanite with a low degree of HT overprint) were selected (Fig. 5). The fold analysis could not be carried out on the rocks from the pluton aureole because of the scarcity of macroscopic folds. The fold shapes, redrawn from photographs, were transformed by parallel projection onto a plane perpendicular to the fold axis. Two quantitative methods have been applied to quantify the fold shape: the method of Lisle (1997) based on Ramsay's (1967) classification and the harmonic fold shape analysis of Hudleston (1973). The principles of these methods are given in Appendix A.

The method of Lisle is based on the polar projection of the normalized thickness of a folded layer. Each fold can be characterized by a single number (the index F), which expresses the amount of flattening within each fold limb. Class 1 folds are characterized by positive F values (0 to ∞) and these give a measure of the amount of homogeneous flattening perpendicular to the axial plane required to generate this fold shape from a parallel fold (class 1C for $F>1$, class 1B for $F=1$ and class 1A for $0<F<1$). Class 3 folds are folds with strong thinning of the limbs (attenuated folds), typically developed in incompetent layers. These folds are characterized by negative F values (0 to $-\infty$). Lisle (1997) divided the field of class 3 folds into three subfields with fold shape 3B marking the boundary between the newly defined 3A and 3C classes. Class 3B folds are defined as a 'pure' class 3 fold geometry from which the other types (3A and 3C folds) develop by the superposition of flattening strains. Class 3A folds are generated from 3B by flattening in the direction normal to the axial plane and have F values ranging from -1 to $-\infty$. Class 3C folds are the result of flattening parallel to the axial plane and are relatively rare in the nature.

Hudleston's (1973) fold classification, based on the Fourier harmonic analysis of folds, exploits the fact that the geometry of a quarter wavelength is sufficient to characterize that of the whole fold. The shape is approximated in terms of its harmonics and it is found that the first two odd harmonics (coefficients b_1 and b_3) are sufficient to adequately describe the fold's profile shape. b_1 expresses the amplitude of the fold profile, b_3 is a measure of the 'angularity' or 'sharpness' of the fold's hinge. For sine waves, $b_3=0$, for box-like folds $b_3>0$ and for chevron-like folds $b_3<0$. The ratios of b_3/b_1 describe a continuous series of shapes between the chevron and box-end members. The method for calculating b_1 and b_3 values is given in Appendix A.

In the present analysis of fold shape, these two methods have been combined by plotting b_1 values (a measure of the active amplification of the fold) against F values (a measure

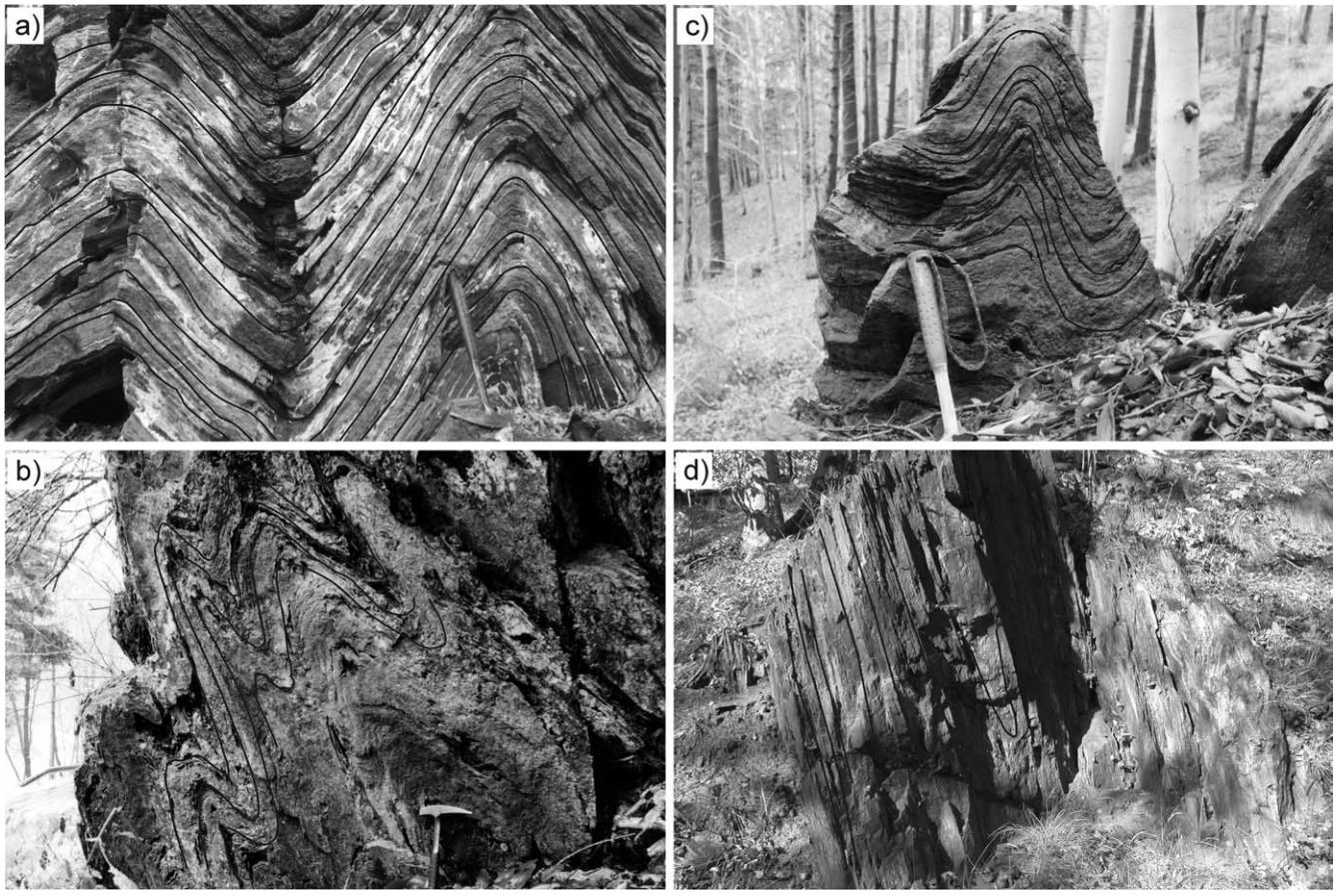

Fig. 5. Field photographs of typical fold shapes: (a) garnet zone, (b) staurolite zone, (c) sillimanite zone and (d) sillimanite zone of the pluton aureole. Chevron folds are typical for the garnet zone (a), flattened folds with high amplitude are characteristic of the staurolite zone (b), and similar folds with rather low amplitudes are present in the sillimanite zone (c). Steep foliation with relic F_3 folds characterize the sillimanite zone in the pluton aureole (d).

of the post buckle flattening). This graph shows the relationship between these two different expressions of shortening. In order to illustrate the geometric implications of this graph we have plotted the fold patterns of the model multilayer sequences given by Ramsay and Huber (1987, pp. 414–415) (Fig. 6). This shows clearly the effect of the viscosity ratio (μ_1/μ_2), layer thickness ratio ($n=d_1/d_2$) and the amount of superimposed strain on the folds position on the graph. Folded incompetent layers plot in the left half of the diagram and the slope of the data points shows the strong negative correlation between the b_1 and F parameters. Folded competent layers plot in the right half of the diagram and the steeper slope of the data point trend shows a less pronounced positive correlation between the b_1 and F parameters (Fig. 6).

We have used these plots as standards with which we compared the plots representing the natural folds from the study area. In addition to the qualitative estimate of the viscosity contrast and the proportion of incompetent to competent fraction, we can deduce semi-quantitatively the active amplification of the buckle fold and the amount of post-buckle shortening. The histograms of the F values and b_3/b_1 ratios for each of the folds studied are given in Fig. 7.

4.2. Quantitative analysis of fold styles in the garnet zone

The post peak metamorphic folds in the eastern part of the massif, i.e. in the garnet zone, display only a small variation in shape. The post buckle flattening is small, as documented by relatively low positive values of F (0.8–3) (Fig. 7a), which approximates to a parallel or weakly flattened parallel fold. Very few folds in this domain belong to class 3A, i.e. folds that exhibit relatively small negative values of F (Fig. 7a). The dominance of class 1B (i.e. parallel) folds is important as it documents that active buckling played a major role during the fold amplification and that post-buckle flattening was subordinate. The shapes acquired from the harmonic Fourier analysis lie between chevron and sine wave, as can be seen from the histogram of b_3/b_1 (Fig. 5a), which has an average value of $b_3/b_1=-0.05$. The absolute values of both F and b_1 are low ($F_{max}=3$; $b_{1max}=3$), suggesting a low amount of deformation of the analysed rocks. A comparison of the measured fold shapes plotted on the b_1 vs. F diagram with the model multilayer sequences (Fig. 6) indicates that the field examples show a close resemblance to model folds (type 5, i.e. folds characterized by a high viscosity ratio (μ_1/μ_2)

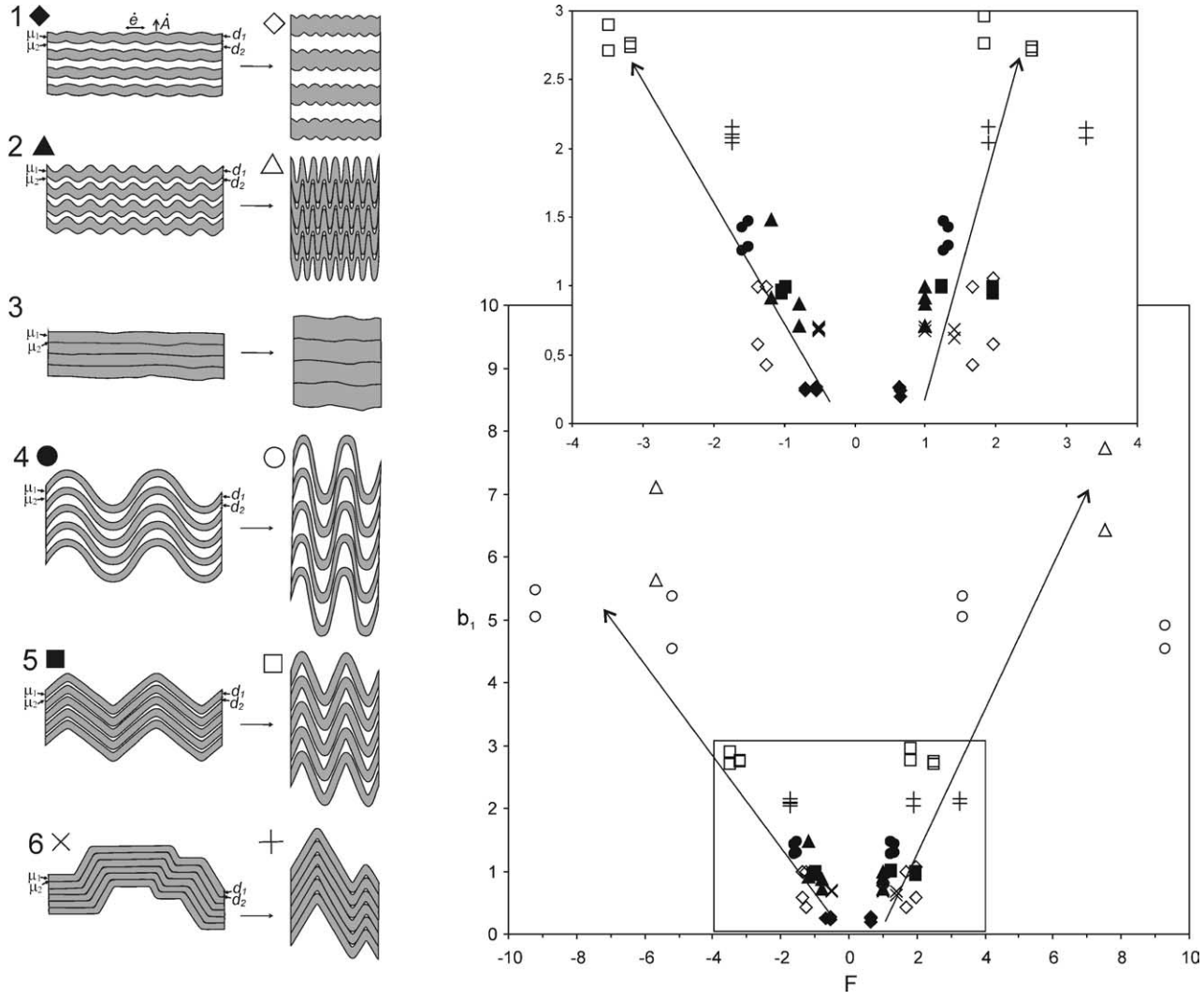

Fig. 6. The position of representative multilayer sequences (modified after Ramsay and Huber (1987, pp. 415–416)) in the diagram b_1 vs. F. The relatively competent layers are dark in colour. Corresponding symbols are given to the left of the schematic drawings; open symbols represent the more deformed stage. The boxed area (F from 4 to −4 and b_1 from 0 to 3) has been enlarged. The properties of the multilayer sequences are (following Ramsay and Huber, 1987): (1) μ_1/μ_2 is low, n (the number of layers) is high, $\dot{A}$ (fold amplification rate) is low, $\dot{e}$ is high; (2) μ_1/μ_2 is low, n is moderate, $\dot{A}$ is moderate, $\dot{e}$ is moderate; (3) μ_1/μ_2 is low, n is low, no characteristic initial wavelength is established; (4) μ_1/μ_2 is high, n is high, $\dot{A}$ is high, $\dot{e}$ is low; (5) μ_1/μ_2 is high, n is moderate, $\dot{A}$ is high, $\dot{e}$ is low. (6) μ_1/μ_2 is high, n is low, $\dot{A}$ is high, $\dot{e}$ is low. Multilayer sequence (3) is missing in our diagram because no folding occurs and the deformation is predominantly layer parallel shortening. (a) and (b) in the text refer to the less and more deformed stages, respectively.

and moderate n (d_1/d_2) values). This fold assemblage has geometry close to that of chevron folds and is characterized by high fold amplification and a low degree of post-buckle flattening.

4.3. Quantitative analysis of fold styles at the staurolite zone

The histogram of F indexes for the post peak metamorphic folds in the staurolite zone (Fig. 2) shows that the folds of class 1B ($F=1$) are no longer present in the central part of the massif (Fig. 7b). Class 1C folds are the most common with F values ranging between 1 and 5 with an average value around 4. There are a number of folds belonging to class 3A, with F values ranging from −10 to −1 with an average of around $F=-4$. These F values indicate that a high amount of post-buckle flattening occurs in both the competent and incompetent layers. Three peaks can be distinguished in the histogram of the b_3/b_1 ratio. One maximum is situated close to the chevron shape, a second is close to the sine wave and the third one lies between the shapes of a parabola and a semi-ellipse (Fig. 7b). However, the majority of the folds are situated between the chevron and sine wave shapes. This shape diversity indicates that fold geometries characteristic of both competent and incompetent materials occur. In the context of the mineral fabric in which these folds develop, this indicates that there are compositional and modal differences implying competence contrasts between layers. The diagram b_1 vs. F also demonstrates that the amphibolites in this zone have suffered an important amount of deformation, which is

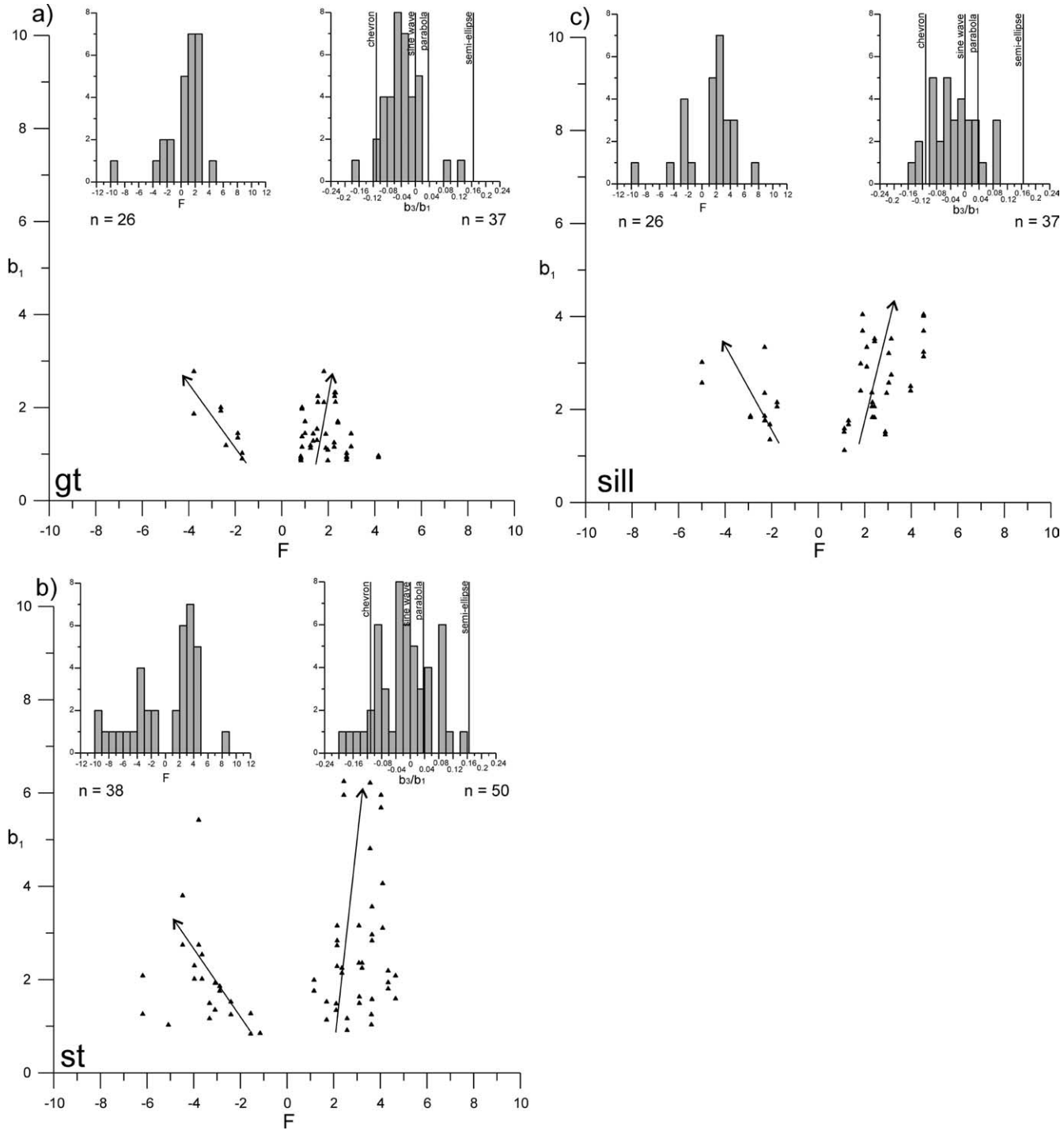

Fig. 7. Graphs of the fold analysis b_1 vs. F with the inset histograms of F and b_3/b_1 coefficients: (a) garnet zone; (b) staurolite zone; (c) sillimanite zone. Typical fold shapes (sine wave, parabola etc.) expressed by the ratio of b_3/b_1 (Hudleston, 1973) are depicted as vertical lines. See text for further discussion.

documented by higher values of the b_1 and F coefficients (Fig. 7b). This fold assemblage corresponds to that of model 5b (Fig. 6) a multilayer sequence marked by high viscosity ratio (μ_1/μ_2) and moderate n (d_1/d_2) values. This implies that high fold amplification and an important post-buckle flattening developed in both competent and incompetent layers. These folds can be regarded as a more deformed equivalent of the fold assemblage observed in the garnet zone (cf. Fig. 7a and b with Fig. 6—model fold types 5a and 5b).

4.4. Quantitative analysis of fold styles in the sillimanite zone

Within the sillimanite zone (Fig. 7c) most of the folds are of class 1C and have F values that are concentrated between

1 and 5 with an average value of around 3. Very few class 3A folds are present. This indicates the important fact that there are relatively few incompetent layers and that a high degree of post buckle flattening has occurred (as indicated by the absence of parallel folds). The broad histogram of the b_1/b_3 ratios, with no unequivocal peaks, reveals that the average fold shape approximates to that of a sine curve. The graph of b_1 vs. F (Fig. 7c) confirms the low number of class 3A folds and the dominance of class 1C. It can be seen from this diagram that class 1C folds ($F>1$) have a low range of b_1 values (between 1 and 4). In addition, we observe a positive correlation between the F and b_1 parameters. The implications of these observations are that although the fold amplification increases with the degree of post-buckle flattening, the maximum value of amplification is relatively low. The measured fold assemblage may be compared with the model folds of type 2b in Fig. 6, which indicate a low viscosity ratio (μ_1/μ_2) and a moderate value of n (d_1/d_2). Compared with the folds in the staurolite zone where high amplification and low post-buckle flattening dominate, in the sillimanite zone we observe limited amplification and pronounced post-buckle flattening. This indicates a change from folding dominated by active amplification (in the staurolite zone) to dominantly passive fold amplification in the sillimanite zone. We interpret this as reflecting an important change in the rheological properties of the folded material rather than the result of differing amounts of finite strain.

4.5. Active buckling vs. post buckle flattening in the studied folds

The fold geometries were examined in order to determine the relative importance of active buckling and post-buckle flattening across the metamorphic zones of the studied amphibolite unit. It has been shown that in the garnet zone fold amplification was dominated by active buckling with only a small contribution from post-buckle flattening. In the staurolite zone, although the folds have also experienced a high degree of amplification, this involved both active buckling and post-buckle flattening. By comparing these results with those obtained from the model folds it can be argued that the folds in the staurolite zone are the equivalent of those in the garnet zone (model fold types 5a and 5b) but have experienced a higher degree of finite strain. In the sillimanite zone the folds show a relatively low amplification but important post-buckle flattening even though field observations suggest that the strain intensity of these folds and those of the staurolite zone are very similar. It is concluded that the dominance of flattening in the folds developed in the sillimanite zone, indicating that the folding was dominated by passive amplification as opposed to that which occurred in the garnet and staurolite zones.

5. Quantitative analysis of rock anisotropy

In order to understand more fully the results of the mesoscopic fold analyses discussed above, it is useful to study the petrofabrics of the folded units. The main goals of this study are to evaluate the mechanical anisotropy of folded systems and to determine the micro-deformational mechanisms associated with folding.

5.1. Methods of quantitative microstructural analysis

Approximately 100 thin sections, collected from all three metamorphic zones, have been studied in an attempt to show the relationship between the microstructures and the folding. Quantitative microstructural analysis has been applied to eight representative samples collected from the garnet, staurolite and sillimanite zones and from the granite aureole. Two thin sections, cut perpendicular to the F_3 fold axes (*YZ* sections), were taken from the fold hinge and fold limb in each zone, respectively. As noted above, macroscopic folds are only present in the garnet to sillimanite zones. The degree of transposition of the original metamorphic fabric within the contact aureole was so high that the macroscopic folds are preserved only in domains with high lithological contrast. However, relics of rootless microscopic folds can be seen in massive amphibolites in thin sections and, in this zone, it is these that are analysed from a microstructural point of view.

A quantitative microstructural analysis of grains and grain boundaries was carried out on the representative samples by tracing and digitising the outlines of individual grains using the ESRI ArcView 3.2 Desktop GIS environment. The map of grain boundaries was generated using ArcView extension Poly (Lexa, 2003). These data have been treated by MATLAB™ PolyLX Toolbox (Lexa, 2003) in which grain boundary and grain SPO were analysed using the moments of inertia ellipse fitting and eigen-analysis of the bulk orientation tensor techniques (Lexa, 2003). Digitised drawings of representative samples are shown in Fig. 8 and the results from the quantitative microstructural analyses are presented in Table 1. The grain size of the minerals was calculated in terms of their Ferret diameter and the resulting grain size distributions were statistically evaluated. The grain size statistics are summarized in Fig. 9, which shows median values and the quartile difference of the Ferret diameters. In addition, a method of determining the orientation of grain boundaries and grain shapes, using the eigen-analysis technique, was applied in an attempt to quantify the bulk rock anisotropy. The results of the analysis of the bulk SPO of grains vs. their aspect ratio (R) are presented in Fig. 10. Grain boundary preferred orientation (GBPO) is presented using a diagram of eigenvalue ratios ($r=e_1/e_2$) and the orientation of the largest eigenvector of the different types of grain boundaries (Fig. 11).

The grain size analysis is a powerful technique for

describing the degree of grain coarsening related to the intensity of metamorphism (Kretz, 1994). Moreover, in polymineralic tectonites the relative grain size distribution for different minerals may indicate the degree of strain–stress partitioning (Handy, 1990; Schulmann et al., 1996). The SPO and elongation of minerals with a low degree of crystallographic anisotropy is generally attributed to the amount of strain in a rock (recrystallized quartz, calcite and feldspar). However, the degree of elongation of strongly anisotropic minerals, such as amphiboles, reflects the degree of metamorphism rather than the degree of strain. Consequently a typical feature of amphiboles is the decrease of axial ratio with increasing metamorphic grade (Brodie and Rutter, 1985). Although the degree of GBPO is the factor most affiliated to the microstructural anisotropy, it is necessary to discuss all of the above-mentioned parameters in order to evaluate the bulk mechanical anisotropy of the rock.

5.2. Grain size distribution

The grain size is expressed as the Ferret diameter of the grain section without stereological corrections. The grain sizes of amphibole and plagioclase show slightly different evolutionary trends (Fig. 9). In the limbs (full symbols), amphibole grain size decreases from 31 to 21 μm from the garnet to the staurolite zone, respectively. The size then increases with increasing metamorphic grade via sillimanite zone reaching 80 μm in the contact aureole of the granite. The grain size distribution of amphiboles in the hinge zones (open symbols) shows a similar trend but the grain size differences between the metamorphic zones are not as high as in the fold limbs. The amphiboles from the fold hinges in the contact aureole (median value 43 μm) are slightly smaller than those from fold hinges in the sillimanite zone (median value 46 μm).

In the limbs, dynamically recrystallized plagioclase has the same grain size in both the garnet and staurolite zones (median value 17 μm). The grain size then increases with increasing metamorphic grade up to a median value of 65 μm in the contact aureole. As with the amphiboles, the grain size is always smaller in the fold hinges reaching a maximum median value of 35 μm in the contact aureole. Both the average grain size of amphibole and the variance are slightly higher than those of plagioclase for all metamorphic zones.

In the garnet zone, amphibole shows a larger grain size and grain size spread than plagioclase (Fig. 9). Moving to the staurolite zone the grain size of the amphiboles decreases, resulting in a decreasing difference in grain size distribution between the plagioclase and amphiboles. The main characteristics of the sillimanite zone are the increase in grain size of both minerals with respect to the previous zones coupled with an increase in difference of grain size distributions. Within the contact aureole the grain size distributions of coarse-grained plagioclase and amphibole become equal.

5.3. Aspect ratio and shape preferred orientation

The microstructures of the fold limbs are characterized by a strong SPO of amphibole grains as well as a high average aspect ratio ($R=2.05$, 2.17 and 2.03 in the garnet, staurolite, and sillimanite zones, respectively) (Fig. 10). Only in the highest metamorphic grade does the SPO decrease, together with the aspect ratio (down to $R=1.57$). Plagioclase displays the same trend as the amphibole but the absolute values of their aspect ratios and SPO are noticeably lower ($R=1.46$, 1.64 and 1.59 in the garnet, staurolite and sillimanite zones, respectively). As with the amphiboles, the aspect ratio and SPO of the plagioclase decreases in the contact aureole ($R=1.49$, i.e. similar to the R value of amphibole in this zone).

The SPO of amphibole in the hinge zones shows a complex evolution. In the garnet zone the SPO is still high, but the aspect ratio is rather low ($R=1.81$). In the staurolite zone both the SPO and the aspect ratio ($R=1.89$) decrease with respect to the limb zone. In contrast the fold hinges in the sillimanite zone are associated with rather high SPO and very high aspect ratio with respect to the previous zone ($R=2.36$). Within the contact aureole it is found that the SPO of amphibole and the aspect ratio ($R=1.60$) diminish in the hinge areas of the microfolds. A similar trend can be observed in the plagioclase ($R=1.48$, 1.53, 1.76 and 1.41 for the garnet, staurolite, sillimanite zones and the contact aureole, respectively).

5.4. Grain boundary preferred orientation

A study of the evolution of amphibole–amphibole grain boundary preferred orientation (GBPO) shows two important trends. The first is the GBPO in the fold limbs which, apart from the staurolite zone, decreases with increasing metamorphic grade ($r=2.12$, 2.39, 1.76 and 1.23 for the garnet, staurolite, sillimanite zones and the contact aureole, respectively) (Fig. 11). The second trend shows that in the garnet and staurolite zones the GBPO in the hinge domains is at a high angle to that of the axial plane representing S_3. It can be seen that in the garnet and staurolite zones the degree of GBPO decreases noticeably in the hinge areas of folds compared with the limb areas ($r=1.47$ and 1.43, respectively). In contrast, in the sillimanite zone, the GBPO in the hinge zone becomes parallel or sub-parallel to the axial plane (S_3) and shows the same intensity ($r=1.7$) to that in the limbs. Similarly, in the contact aureole, the GBPO in the hinge zones shows parallelism to the axial plane (S_3), and has a similar intensity ($r=1.22$) to that on the limbs.

The r values for plagioclase–plagioclase boundaries are weak for all the zones (1.06–1.21; see Fig. 11 and Table 1) indicating a very weak or even a lack of GBPO. In contrast, the amphibole–plagioclase GBPO, which is controlled by

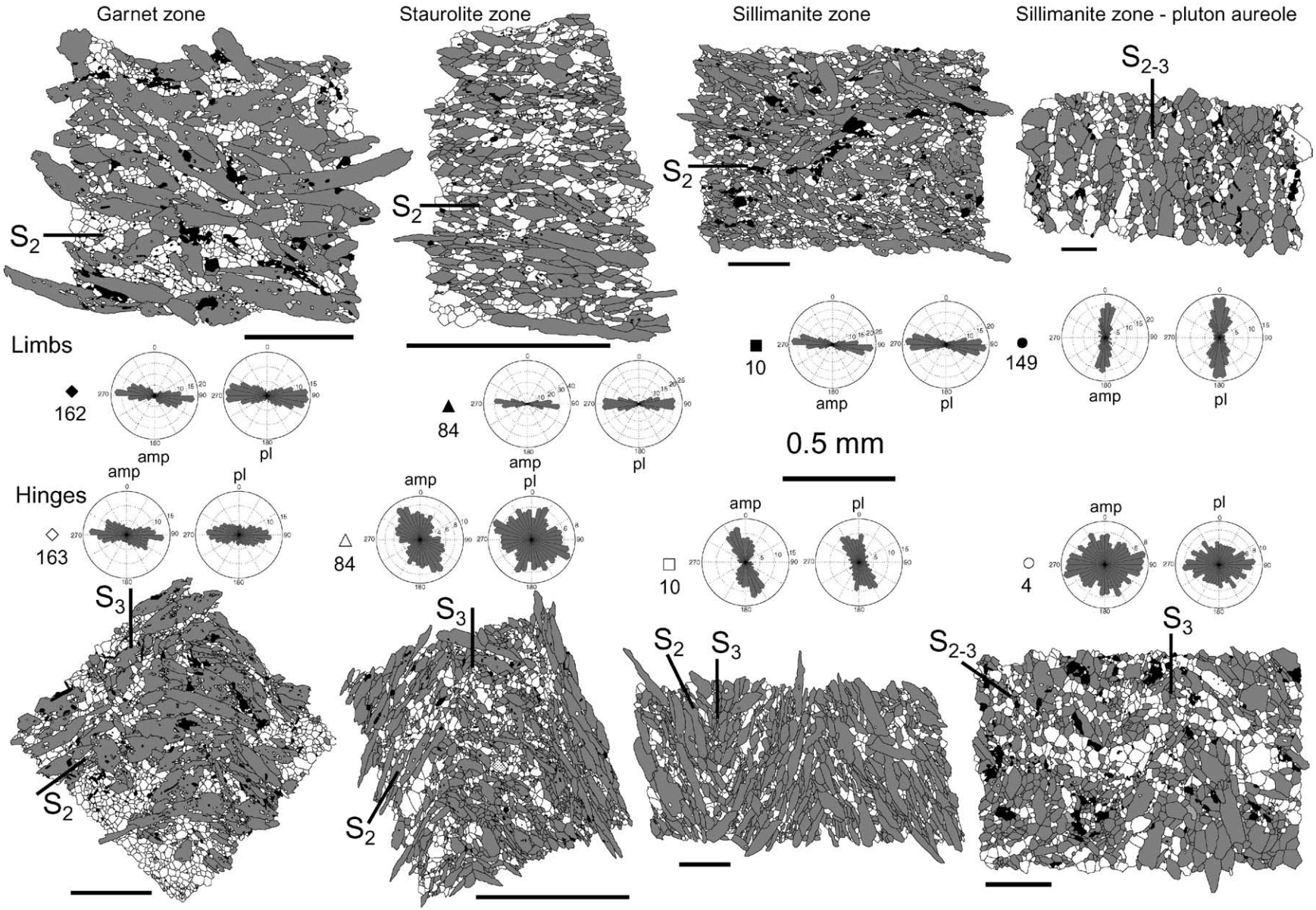

Fig. 8. Typical microstructures from the four metamorphic zones, redrawn and digitized in the ArcView GIS environment. The rose diagrams represent grain long axis distribution. Full symbols correspond to fold limbs, open symbols to fold hinges. These symbols have the same significance in Figs. 9 and 11. The minerals can be identified as follows: plagioclase—white; amphibole—medium grey; sphene + ilmenomagnetite—black; quartz—vertically hatched; calcite—dotted; clinopyroxene—light grey.

Table 1
Statistical values of the quantitative textural analysis

Zone		Grt		St		Sil		Sil (pluton aureole)	
Sample		162	163	84	84	10	10	149	4
		Limb	Hinge	Limb	Hinge	Limb	Hinge	Limb	Hinge
GBPO	Pl–pl	1.06	1.10	1.21	1.21	1.25	1.12	1.10	1.22
Eigenvalue $r = e_1/e_2$	Amp–amp	2.12	1.47	2.39	1.43	1.76	1.70	1.23	1.22
	Amp–pl	1.45	1.17	1.95	1.26	1.48	1.52	1.33	1.08
Eigenvector orientation (°)[a]	Pl–pl	−25	−74	22	88	−9	−65	28	83
	Amp–amp	−11	−22	−3	−76	−11	−77	74	−83
	Amp–pl	−16	−2	−4	89	−14	−78	91	−73
SPO	Pl	1.21	1.06	1.57	1.25	1.42	1.44	1.23	1.16
Eigenvalue r	Amp	2.39	1.57	3.06	1.44	2.16	1.88	1.44	1.31
Eigenvector orientation (°)[a]	Pl	−16	−38	1	−90	−9	−81	89	−90
	Amp	−11	−3	−6	−88	−15	−79	79	−86
Aspect ratio (median)	Pl	1.46	1.48	1.64	1.53	1.59	1.76	1.49	1.41
	Amp	2.05	1.81	2.17	1.89	2.03	2.36	1.57	1.60
Grain size—Ferret diameter									
Median (μm)	Pl	17	22	17	15	39	28	65	35
	Amp	31	33	21	20	64	46	80	43
Q_1 (μm)	Pl	11	14	10	10	27	20	36	21
	Amp	16	18	13	13	38	29	45	29
Q_3 (μm)	Pl	25	34	25	21	52	39	114	53
	Amp	75	59	35	32	104	79	130	65
$Q_3 - Q_1$ (μm)	Pl	14	20	15	12	25	19	79	33
	Amp	59	41	22	19	66	49	85	37

[a] Positive values are oriented anticlockwise with respect to the horizontal.

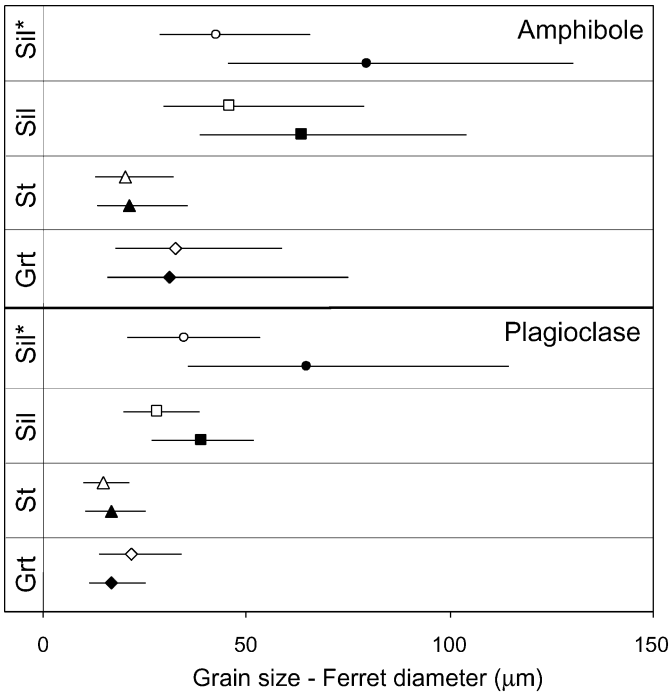

Fig. 9. Plot of amphibole and plagioclase median of Ferret diameter and variances for all the metamorphic zones studied. Full symbols correspond to fold limbs and open symbols represent hinge areas. Samples from the pluton aureole are assigned as Sil*.

the difference between the grain size of the large elongate grains of amphibole and small grains of plagioclase as well as by the SPO of the amphibole, is higher. The highest GBPO for these boundaries is developed in the limb zones of the folds in the staurolite zone ($r=1.95$). The degree of GBPO is low in the limb zones of folds in the garnet and sillimanite zones ($r=1.45$ and 1.48, respectively) and further decreases to $r=1.33$ in the contact aureole. In the hinge regions the GBPO of plagioclase–amphibole boundaries is very low in the garnet, staurolite zones and contact aureole ($r=1.17$, 1.26 and 1.08, respectively; Fig. 11). It is only in the hinge zones of the folds in the sillimanite zone that the GBPO of this boundary exceeds 1.5 ($r=1.52$).

5.5. A comparison of the microstructures in the hinge and limb areas for folds from the different metamorphic grades

The analysis of the limb areas of the folds in the garnet zone reveals a large grain size and aspect ratio difference between the amphiboles (elongate and large) and plagioclase (sub-equant and small) (Figs. 9 and 10). This work also shows a relatively small SPO and GBPO for plagioclase compared with strong SPO and GBPO for amphibole. This microstructure represents a network of large amphibole crystals surrounding pockets of fine-grained plagioclase. In the hinge regions of folds in the garnet zone the amphiboles are oriented at high angles to the axial plane. Compared with the limb there is a decrease in the aspect ratio, grain size, SPO and GBPO of both minerals.

In the limbs of the folds in the staurolite zone both the amphiboles and the plagioclase display a very intense SPO, high aspect ratio and a strong GBPO coupled with a decreasing difference in grain size between the two minerals compared with the fold limbs in the garnet zone (Figs. 9–11). This reflects the fact that both minerals form interconnecting aggregates. The hinge zone microstructure, like that in the garnet zone, is marked by rotation of the fabric into an orientation at a high angle to the fold axial plane and, compared with the limbs, the mineral aspect ratio, grain size, SPO, and GBPO are all reduced.

The sillimanite zone and the contact aureole both show an increase in grain size for both minerals compared with the garnet and staurolite zones (Figs. 9–11). However, the main difference is the parallelism of the mineral preferred orientation in the hinge zones with the fold axial plane, which is expressed by both the SPO and the GBPO (Figs. 8 and 11). This is connected with an increase in aspect ratio for both plagioclase and amphibole in the hinge compared with the limb. The other important feature is the similar GBPO for like–like and unlike boundaries for both the hinge and limb zones. The only difference between the sillimanite zone and contact aureole is a weakening of the SPO and GBPO in the latter where the aspect ratio of both minerals approaches 1. The distribution of amphibole and plagioclase aggregates in the limbs is rather random in the sillimanite zone and tends to be layered in the contact aureole.

In summary, we note that the rocks of the study area fall into two distinct groups. Those in the garnet and staurolite zones, which show mineral preferred orientation in the hinge zone at a high angle to the fold axial plane and to the

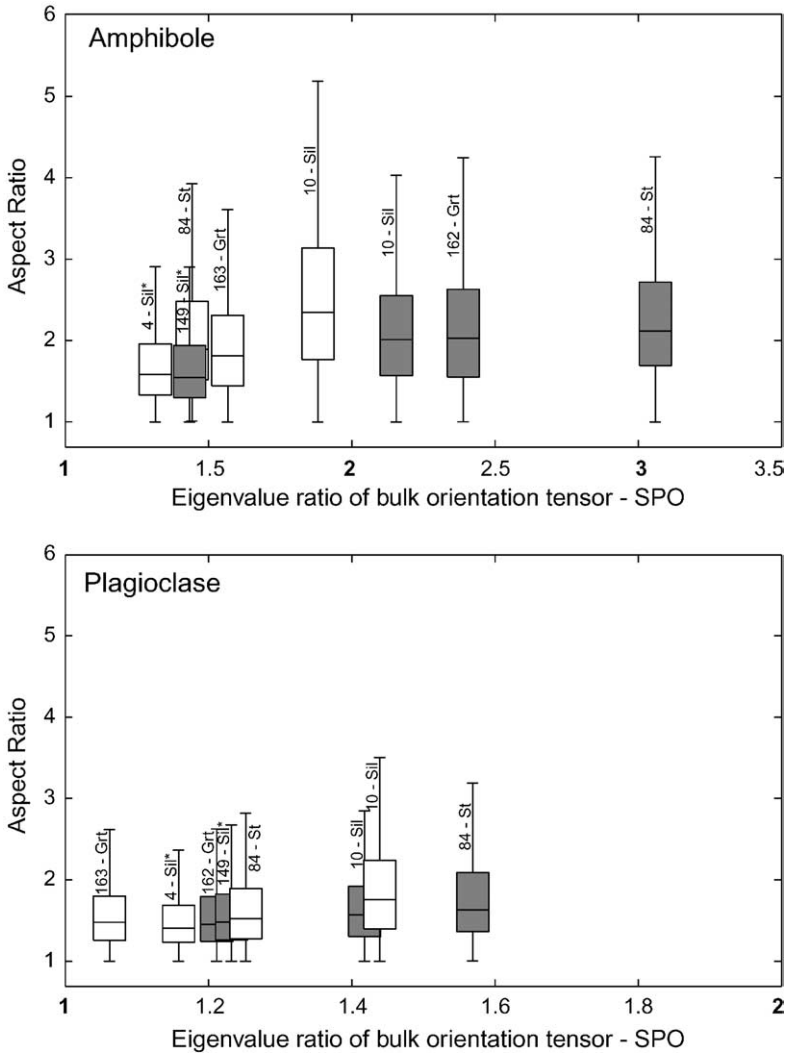

Fig. 10. The plot of grain shape preferred orientation (SPO) of amphibole and plagioclase displaying the weighted ratio of the eigenvalues of inertia. The results are summarized in a boxplot-type diagram of aspect ratios vs. eigenvalue ratio of bulk matrix of inertia of the individual minerals. The individual boxes show the median, first and third quartiles of the aspect ratio. The 'whiskers' represent statistical estimates of the data range. Outliers are not plotted. Boxes of the limbs are shaded while those of hinge areas are white. The number of the analysed sample is indicated for each zone. Samples from the pluton aureole are assigned as Sil*.

SPO of amphibole and plagioclase on the limbs, and those in the sillimanite zone and contact aureole, which show mineral preferred orientation in the hinge zone sub-parallel to the axial plane.

6. Discussion

In this paper we have attempted to use the theory of buckling of multilayers and the theory of buckling of mechanically anisotropic materials to explain the folding mechanisms of some natural folds, which show lateral variations in their shape. The folds are developed in a rock unit of constant mineral composition but which exhibits a lateral variation in rock microstructure related to metamorphic grade. Systematic variations in fold shapes across the whole profile suggest that the original variations in rock protolith are less important for folding mechanisms than the metamorphic recrystallization associated with development of mineral fabrics prior to the folding event.

6.1. Competence contrast vs. mechanical anisotropy

The question arises as to whether the differences between the fold styles in the garnet and staurolite zone, and folds in the sillimanite zone, are the result of differences in the mechanical anisotropy of the mineral fabric or of rheological variations between adjacent layers. As is discussed in the following section, an inspection of Figs. 6 and 7 can help answer this.

The buckling behaviour of a multilayer is controlled by the ratio of the competencies, e.g. the viscosities (μ_1/μ_2) of the competent and incompetent layers and their relative thicknesses (e.g. Ramberg, 1963). The most important

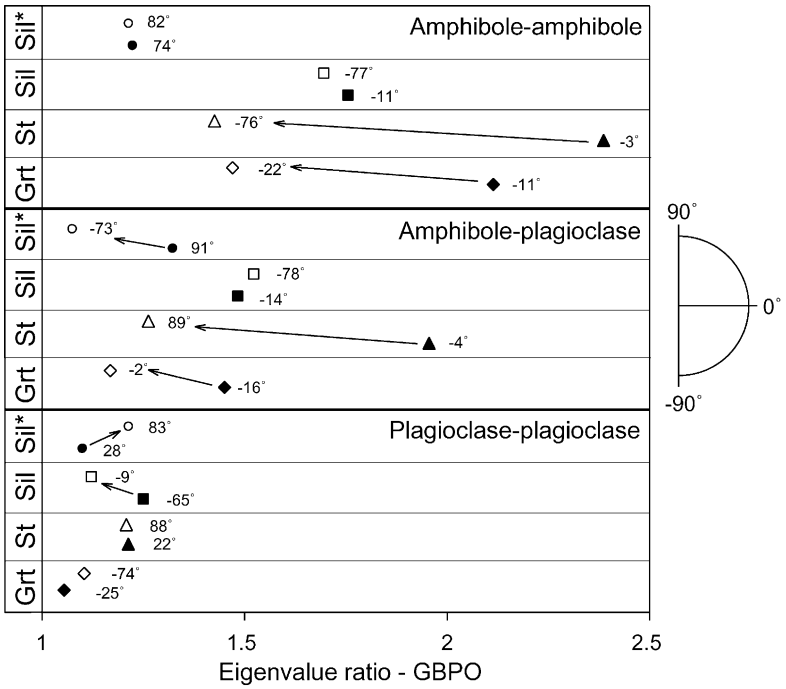

Fig. 11. Plot of grain boundary preferred orientation (GBPO) of amphibole–amphibole, amphibole–plagioclase and plagioclase–plagioclase boundaries displaying weighted ratio of eigenvalues of inertia. The numbers represent the orientation of the eigenvector V_1 of GBPO with respect to the horizontal. Positive values indicate anticlockwise deviation. Samples from the pluton aureole are labelled Sil*.

factor controlling the mode and style of folding of a mineral fabric is the mechanical anisotropy of the material and this is defined by the ratio of two moduli, one a measure of the resistance to layer or fabric parallel compression (M) and the other to the resistance to shear in the same direction (L).

It can be shown that there is a direct link between the anisotropy (M/L) and the competence contrast of a bilaminate (μ_1/μ_2) (see Price and Cosgrove, 1990) and this allows one to use both theories to study folding behaviour. By analysing the geometries of the studied folds it is possible to determine which of the two theoretical approaches is more appropriate. As shown earlier, the low F values of the folds from the garnet (low b_1) and staurolite zones (high b_1) are similar to those in the range type 5a and 5b to type 4b (Fig. 6). The trend of the arrows in Fig. 7b (which indicates the ratio of active buckling amplification and fold flattening in the staurolite zone) is comparable with the trends indicated in Fig. 6 for a multilayer (type 5b) with a high competence contrast between adjacent layers. The construction of the dip isogons for the folds from this zone shows alternations of layers with different geometries (classes 1B and 1C alternating with class 3) and different curvature profiles of the hinge regions (Fig. 12), a pattern compatible with the folds of type 5b. Using the classical theory of Ramberg (1963), this pattern can be interpreted in terms of folding of a multilayer sequence marked by alternation of layers with a high competence contrast.

However, as was shown above, the garnet zone amphibolites are more or less compositionally homogeneous and do not show distinct compositional layering. Inspection of Fig. 7a shows that the folds in the garnet zone could be considered to represent the early stages of active and passive amplification observed in the staurolite zone. However, there is a marked difference in the density of the data relating to the 'competent' and 'incompetent' members of the multilayer. When the pattern of dip isogons for a representative fold profile for these folds is examined (Fig. 12), it can be seen that there is an important increase of fold flattening component resulting in a convergence of shapes (and therefore dip isogon patterns) of adjacent layers.

A comparison of the natural data from folds in the sillimanite zone (Fig. 7c) with the model folds in Fig. 6 shows that the best fit is with type 2b folds. This geometry is traditionally interpreted as indicating a bilaminate with a low competence contrast. However, we note the strong asymmetry in the density of points indicating a lack of incompetent 'layers'. This is confirmed by inspection of the dip isogon pattern of representative folds from this zone (Fig. 12). Although the pattern shows alternations of fold shapes of class 1C with those of class 3, it is obtained by analysing 'layers' that are composed of several units. The absence of alternations of clearly defined individual layers combined with the high degree of flattening and relatively low fold amplification indicate that this system approximates more closely to the model analysed by Biot than to a bilaminate.

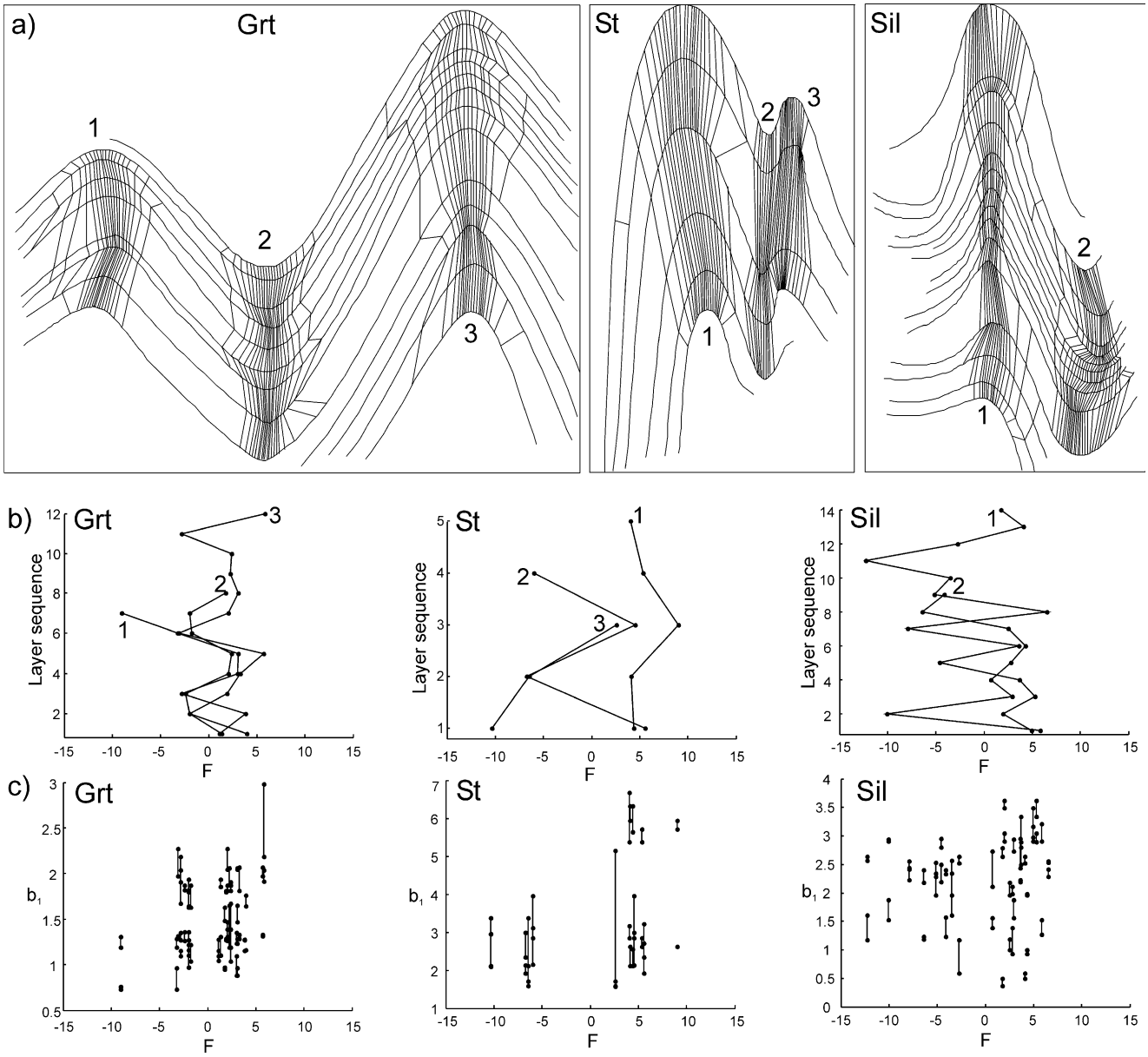

Fig. 12. Selected fold assemblages from the garnet, staurolite and sillimanite zones, respectively. (a) Dip isogon patterns. (b) Graphs showing the changes in F (degree of fold flattening) across successive folded layers for each fold assemblage. (c) b_1 vs. F plots constructed for the presented folds showing the relative importance of fold flattening and active fold amplification.

6.2. Interpretation of the deformation micro-mechanisms associated with folding

Experimental work on amphibole and plagioclase as well as field observations have shown that the former mineral is stronger than the latter under the complete range of homologous temperatures (see Brodie and Rutter (1985) for a review). Observations of the microstructures in the hinge zone show that the micro-folding in the garnet zone has been achieved by the bending and fracturing of the strong amphiboles whilst the relatively weak plagioclase recrystallizes and accommodates space modifications associated with the rigid body rotation of the amphibole crystals in a weak matrix by mechanism modelled by Arbaret et al. (2001), for example (Table 2). However, no fracturing or bending of amphiboles is observed in limb zones, which implies that the fabric on the limbs still represents the original, i.e. pre-folding, fabric. Folding of amphiboles in the garnet zone is thus similar to that described from low-grade metasediments and which leads to the occurrence of metamorphic differentiation (Cosgrove, 1976). In this work, Biot's (1961) theory was used to account for the buckling of a greenschist facies mineral fabric made up of a rigid stress supporting framework of mica containing interstitial weak quartz. In the hinge the framework of mica protects the quartz from the buckling

stress but on the limbs it does not. The resulting stress gradients cause the migration of quartz from the limb to the hinge and mica from the hinge to the limb.

Microstructural examination of the rocks in the present study area shows an analogous situation in the amphibole plagioclase rock. The resulting stress gradients established in both the amphibole and the plagioclase cause a migration of plagioclase to the hinge and amphibole to the limbs, leading to metamorphic differentiation.

We suggest that this process operated in the hinge zones of some macrofolds leading to their thickening. Because of strain compatibility, this hinge thickening develops in alternating layers, thus producing patterns similar to the folding of bilaminate (Fig. 12).

In the hinge zones of folds in the staurolite zone a conspicuous reduction in the grain size of the amphiboles with respect to the limb zones can be observed. This is locally connected with the reorientation of amphibole fragments, and we interpret this microstructure as being the result of the fracturing and rigid body rotation of amphiboles as described by Nyman et al. (1992). The dynamically recrystallized plagioclase in the hinge zones also shows a decrease in grain size with respect to the limb. In the hinges, both minerals have similar grain size, low aspect ratio, very weak SPO and GBPO and exhibit an important degree of mixing. We suggest that these features may stimulate a change in deformation mechanism in these domains and that in the highly attenuated folds the fracturing of amphiboles and the dynamic recrystallization of plagioclase switch to a type of granular flow facilitating the development of high strain intensities in these areas (Table 2). The changeover from dislocation creep dominated flow to granular flows connected with a reduction of grain size and the mechanical mixing of minerals has been described by several authors in greenschist facies metabasite mylonites (e.g. Stünitz, 1993; Berger and Stünitz, 1996). As with the folds in the garnet zone we argue that the fabric on the limbs of the folds in the staurolite zone represents the original, pre-fold fabric.

In contrast to the garnet and staurolite zones no bending or fracturing of the amphibole lattice was noted in the hinge zones of folds in the sillimanite zone. Instead the fold hinge areas in the sillimanite zone display crossover growths of amphiboles and straight, well-equilibrated grain boundaries of all minerals. In addition, the amphibole grains show no signs of internal deformation and the grain size is always higher than that observed in the garnet and staurolite zones. All these criteria indicate that these grains developed by the mechanism of nucleation and possibly syn-deformational growth (Vernon, 1976; Rosenberg and Stünitz, 2003). The plagioclase also shows well-equilibrated grain boundaries meeting at triple point junctions and an almost uniform distribution in the rock, features consistent with the high-grade crystallization of amphiboles and plagioclase (Brodie and Rutter, 1985). Comparison of the mineral microstructures of the hinge zones and the limbs shows that the hinge zones display higher aspect ratios, smaller grain sizes, similar SPO and like–like and unlike GBPOs (Table 2). This implies that, during the development of the folds, recrystallization occurred simultaneously in both the hinge zones and the limbs, producing an increase in elongation of the original crystals in the hinge zone. This is because the grains in both the limb regions and the hinge regions are parallel to the axial plane, i.e. are perpendicular to the largest principal compressive stress axis. This resulted in an increase in aspect ratio by the process of heterogeneous dissolution accompanied by recrystallization and grain growth, the mechanism of schistosity transposition well known in high grade schists and described by a number of authors (see Passchier and Trouw (1996, fig. 4.17) for a review). Unlike the folds in the garnet and staurolite zones where we consider that the fabric on the fold limbs represents the pre-folding microstructure, in the sillimanite zone it is modified by dissolution and growth process.

In the contact aureole a similar type of microstructural pattern to the sillimanite zone occurs but it is marked by a complete loss of SPO and GBPO coupled with an important grain size increase (Table 2). These features are consistent with there having been an important contribution from high grade “static” recrystallization in both the hinge and limb domains. However, we emphasise that one can still observe smaller grain sizes and aspect ratios for both amphibole and plagioclase in the hinge zones compared with the limbs.

7. Conclusions

A summary of the fold analysis and the microstructural studies supporting the fold mechanics models is given in Table 2.

The garnet grade region. The quantitative microstructural analysis of the limb zones in the folds in the garnet zone reveals the possible existence of a stress-supporting network. This type of structure implies a relatively homogeneous stress distribution in the rock (Jordan, 1988), which is controlled by the rheologically resistant amphiboles, with the plagioclase representing only weak pockets that deform to accommodate the deformation imposed by the strong amphibole. This is supported by the large grain size difference between the recrystallized plagioclase and amphibole crystals, which can be interpreted in terms of a stress-supporting network with a high rheological contrast between the plagioclase and amphibole (Handy, 1990). In addition, the microstructural analysis shows that the amphibole stress-supporting framework collapses in the hinge zones by brittle failure. This brittle deformation, which represents an extreme example of strain localization, tends to produce sharp-hinged chevron folds on a grain scale (Fig. 3a and b).

The observed folding mechanism also gives rise to chevron folds on a macroscopic scale indicating that the mechanical anisotropy of the rock was high. To interpret the

Table 2
Summary of parameters derived from fold shape and microstructural analyses in all zones. Used symbols are: A, Amp—amphibole; P, Pl—plagioclase; S—grain size; R—aspect ratio; SPO—shape preferred orientation; GBPO—grain boundary preferred orientation

		Garnet zone				Staurolite zone				Sillimanite zone and pluton aureole			
Folding mechanisms		Active amplification				Active amplification and post-buckle flattening				Passive amplification			
Degree of mechanical anisotropy		Low to medium b_1. Low positive F High mechanical anisotropy				Medium to high b_1. High F Bilaminate				Low to medium b_1. High positive F Low mechanical anisotropy			
Quantitavive microstructure parameters		S	R	SPO	GBPO	S	R	SPO	GBPO	S	R	SPO	GBPO
	Limb	A>P	A>P	A>P	A>P	A=P	A≥P	A≥P	A≥P	A=P	A=P	A=P	A=P
	Hinge	A>P	A>P	A>P	A>P	A=P	A≥P	A≥P	A>P	A=P	A=P	A=P	A=P
Microstructure		Amphibole supported LBF (large elongate and interconnected Amp grains surrounding pockets of fine-grained Pl)				IWL microstructure with low-viscosity contrast (alternation of Pl-rich and Amp-rich aggregates)				Amphibole supported LBF structure with low-viscosity contrast (mixture of Amp and Pl of equal size and aspect ratio)			
Deformation mechanisms		Hinge		Limb		Hinge		Limb		Hinge and limb			
		Amp fracturing		Brittle reactivation of S_2 fabric		Amp fracturing and granular flow of Amp–Pl matrix		Dynamic recrystallization of Pl and ductile flow in Pl-rich layers		Nucleation and syndeformational growth			

isogon patterns (Fig. 12) we propose an explanation of alternations of hinge zones thickened by this mechanism of microfolding with those without any thickening and distinct microstructural changes.

The staurolite grade region. In the limbs of folds generated in the staurolite zone, the pre-folding fabric is marked by fairly well developed, alternating elongate aggregates of plagioclase and amphibole. The intensity of mineral preferred orientation is very strong, as documented by the high aspect ratio and strong GBPO and SPO values. Inspection of the fabric in thin sections (Fig. 3c and d) suggests that this structure approximates to the so-called 'interconnected weak layer structure' (IWL of Handy (1990)) characterized by an alternation of relatively strong amphibole rich domains and relatively weak domains rich in plagioclase. Because the alternating domains differ only in small modal differences in amphiboles and plagioclase this structure represents an IWL structure with a low viscosity contrast as defined by Handy (1994). Such a system possesses the geometrical characteristics of a bilaminate with diffuse boundaries between the layers. In the hinge zones the microfabric shows areas of distributed deformation. During fold development these zones of distributed deformation (granular flow in the hinge zones) would contribute to strain softening in this region leading to continuous amplification of the folds. We note that even if the deformation of the amphiboles is by brittle failure, it results in distributed ductile flow in the highly deformed hinges. Unlike the folds in the garnet zone where probably no slip on the limbs occurred, in the staurolite zone the slip is distributed through the relatively weak plagioclase rich zones increasing the tendency for active amplification of the fold. In addition, on the limbs, because of the presence of relatively weak 'layers', fold amplification can be further assisted by flattening. This is well documented by the dip isogons pattern and the b_1 vs. F graph of Fig. 12.

The sillimanite grade zone. In the sillimanite zone the amphibole and plagioclase show a relatively high aspect ratio connected with a low degree of GBPO of like–like and unlike boundaries. In this zone, unlike the staurolite zone where the plagioclase was interconnected, isolated elongate grains or aggregates of plagioclase surrounded by highly elongate and well-oriented crystals of amphibole occur (Figs. 3e and f and 8). This structure and the flattening of both minerals can be interpreted in terms of a stress-supporting network with a low viscosity contrast between weaker plagioclase and stronger amphibole (Handy, 1990). Thus, in the sillimanite zone, it was the strength of 'weaker' plagioclase that dominated the rheological properties of the system, which therefore acted as a relatively weak, homogeneous material.

In contrast to the garnet zone, where buckling was controlled by localized microfolding and to the staurolite zone where it was controlled by ductile shearing along weak, plagioclase rich zones, no such zones of weakness, which facilitate the active amplification of the folds, are observed in the sillimanite zone. Instead the fold shape analysis shows an importance of post-buckle flattening over active fold amplification. The micro structural analysis of both the limb and hinge areas shows features consistent with homogeneous flattening (i.e. higher aspect ratio and smaller grain size in the hinge domains than in the limbs) an observation entirely consistent with passive amplification of a material with a low mechanical anisotropy.

The contact metamorphic aureole. The deformation in the contact aureole (Figs. 3g and h and 8) is an extreme example of flattening dominated deformation as shown by differences in grain size and grain shapes in the hinge and limb areas. The lack of macroscopic folds in the amphibolites within the aureole is taken as further evidence that the amplification was almost entirely passive.

Acknowledgements

The project was funded by grants of Czech National Grant Agency No. 42-201-204 to K.S. and 42-201-318 to P. Štípská, by Czech Geological Service assignment No. 6327 to P. Mixa, and by a Ph.D. financial support attributed by the French Government to L.B. We thank R. Vernon and D. Grujic for constructive reviews and J. Hippertt for editorial help.

Appendix A

A polar graph aimed to represent the variation of orthogonal thickness t around folded layers was first utilized by Lisle (1997). A fold can be represented by a series of points with polar coordinates ($1/t'$, α), where $1/t'$ is the reciprocal normalized thickness ($t' = t/t_h$, where t_h is the extreme value of t, which is generally situated in the fold hinge), and α is the orientation of the layer tangent. Using this technique, Ramsay's (1967) fold types give rise to various conic sections (ellipses, hyperbolas) in the polar graph with horizontal semiaxis equal to unity (see Lisle, 1997).

Flattening index **F**, or axial ratio of strain ellipse, express the amount of post-buckle flattening superimposed on the parallel fold. We used a numerically stable direct least-square method (Halíř and Flusser, 1998) to fit either ellipses or hyperbolas onto points in a polar graph of normalized thickness. This technique of evaluation of the flattening index **F** poses a robust estimate and is preferred in this work.

The method of analysing fold shapes in terms of the harmonic coefficients of a Fourier series was originally devised by Stabler (1968) and subsequently elaborated by Hudleston (1973).

The most basic and suitable segment of a folded surface for analysis is a 'quarter-wavelength' unit between adjacent hinge and inflexion points. Such a choice of unit leads to a harmonic series consisting only of the odd terms of a sine

series and the fold profile is thus approximated by the equation:

$$f(x) = \sum_{n=1}^{\infty} b_{2n-1} \sin\left(\frac{(2n-1)\pi x}{2L}\right)$$

The first few harmonic coefficients are sensitive parameters of fold shape and most information about the fold shape can be gained from the first two coefficients, b_1 and b_3.

To obtain these coefficients, a 'quarter-wavelength' unit of length L of the fold is divided into equal sectors on a line, which is perpendicular to the axial surface and passes through the inflection point. Pairs of $f(x_n)$ and x_n coordinates are measured at each of these points. A system of linear equations is assembled from pairs $\{x_n, f(x_n)\}$ and solved for unknown coefficients, so

$$\begin{bmatrix} \sin\left(\frac{\pi x_1}{2L}\right) & \sin\left(\frac{3\pi x_1}{2L}\right) & \cdots & \sin\left(\frac{(2n-1)\pi x_1}{2L}\right) \\ \sin\left(\frac{\pi x_2}{2L}\right) & \sin\left(\frac{3\pi x_2}{2L}\right) & \cdots & \sin\left(\frac{(2n-1)\pi x_2}{2L}\right) \\ \vdots & \vdots & \ddots & \vdots \\ \sin\left(\frac{\pi x_n}{2L}\right) & \sin\left(\frac{3\pi x_n}{2L}\right) & & \sin\left(\frac{(2n-1)\pi x_n}{2L}\right) \end{bmatrix} \begin{bmatrix} b_1 \\ b_3 \\ \vdots \\ b_{2n-1} \end{bmatrix} = \begin{bmatrix} f(x_1) \\ f(x_2) \\ \vdots \\ f(x_n) \end{bmatrix}$$

References

Arbaret, L., Mancktelow, N.S., Burg, J.-P., 2001. Effect of shape and orientation on rigid particle rotation and matrix deformation in simple shear flow. Journal of Structural Geology 23, 113–125.

Baratoux, L., 2004. Petrology, deformation mechanisms, and fabric anisotropy of metabasites deformed at natural strain and metamorphic gradient. Ph.D. thesis, Charles University, Prague.

Berger, A., Stünitz, H., 1996. Deformation mechanisms and reaction of hornblende: examples from the Bergell tonalite (central Alps). Tectonophysics 257, 149–174.

Biot, M.A., 1961. Theory of folding of stratified viscoelastic media and its implication in tectonics and orogenesis. Bulletin of the Geological Society of America 72, 1595–1620.

Biot, M.A., 1963a. Stability of multilayer continua including the effect of gravity and visco elasticity. Journal of Franklin Institute 276, 231–252.

Biot, M.A., 1963b. Theory of stability of multilayered continua in finite, anisotropic elasticity. Journal of Franklin Institute 276, 128–153.

Biot, M.A., 1967. Rheological stability with couple stresses and its implication to geological folding. Proceedings of the Royal Society of London, Series A 2298, 402–423.

Brodie, K.H., Rutter, E.H., 1985. On the relationship between deformation and metamorphism, with special reference to the behavior of basic rocks. In: Thompson, A.B., Rubie, D.C. (Eds.), Metamorphic Reactions; Kinetics, Textures, and Deformation. Springer-Verlag, New York, pp. 138–179.

Cháb, J., Žáček, V., 1994. Geology of the Žulová pluton mantle (Bohemian massif, Central Europe). Věstník ÚÚG 69, 1–12.

Chlupáč, I., 1994. Facies and biogeographic relationships in Devonian of the Bohemian massif. Corier Forschungsinstitut Senckenberg 169, 299–317.

Cosgrove, J.W., 1976. The formation of crenulation cleavage. Journal of the Geological Society of London, 132(Part 2, 155–178.

Dubey, A.K., 1980. Late stages in the development of folds as deduced from model experiments. Tectonophysics 65, 311–322.

Dubey, A.K., Cobbold, P.R., 1977. Noncylindrical flexural slip folds in nature and experiment. Tectonophysics 38, 223–239.

Dudek, A., 1980. The crystalline basement block of the outer Carpathians in Moravia—Brunovistulicum. Rozpravy Československé Akademie věd, Rada matematika—prírodní vědy 90, 85pp.

Fletcher, R.C., 1995. Three-dimensional folding and necking of a power-law layer: are folds cylindrical and do we understand why? Tectonophysics 247, 65–83.

Fowler, T.J., Winsor, C.N., 1996. Evolution of chevron folds by profile shape changes; comparison between multilayer deformation experiments and folds of the Bendigo–Castlemaine goldfields, Australia. Tectonophysics 258, 125–150.

Ghosh, S.K., 1968. Experiments of buckling of multilayers which permit interlayer gliding. Tectonophysics 6, 207–249.

Halír, R., Flusser, J., 1998. Numerically stable direct least squares fitting of ellipses. In: Proceedings of the 6th International Conference in Central Europe on Computer Graphics and Visualization, WSCG '98. CZ, Plzeň, pp. 125–132.

Handy, M.R., 1990. The solid-state flow of polymineralic rocks. Journal of Geophysical Research, B 95, 8647–8661.

Handy, M.R., 1994. Flow laws for rocks containing two non-linear viscous phases; a phenomenological approach. Journal of Structural Geology 16, 287–301.

Hobbs, B., 1971. The analysis of strain in folded layers. Tectonophysics 11, 329–375.

Hudleston, P.J., 1973. Fold morphology and some geometrical implications of theories of fold development. Tectonophysics 16, 1–46.

Jehlička, J., 1995. The Žulová Massif in Silesian—its geochemistry and petrogenesis. PhD thesis, Charles University, Prague.

Jordan, P.G., 1988. The rheology of polymineralic rocks—an approach. Geologische Rundschau 77, 285–294.

Kretz, R., 1994. Metamorphic Crystallization. Wiley, New York.

Lexa, O., 2003. Numerical approach in structural and microstructural analyses. Ph.D. thesis, Charles University, Prague.

Lisle, R.J., 1997. A fold classification scheme based on a polar plot of inverse layer thickness. In: Sengupta, S. (Ed.), Evolution of Geological Structures in Micro- to Macro-scales. Chapman & Hall, London, pp. 323–339.

Maluski, H., Rajlich, P., Souček, J., 1995. Pre-Variscan, Variscan, and Early Alpine thermo-tectonic history of the north-eastern Bohemian Massif: $^{40}Ar/^{39}Ar$ study. Geologishe Rundschau 84, 345–358.

Mancktelow, N.S., Abbassi, M.R., 1992. Single layer buckle folding in non-linear materials; II. Comparison between theory and experiment. Journal of Structural Geology 14, 105–120.

Nyman, M.W., Law, R.D., Smelik, E.A., 1992. Cataclastic deformation mechanism for the development of core-mantle structures in amphibole. Geology 20, 455–458.

Oertel, G., Ernst, W.G., 1978. Strain and rotation in a multilayered fold. Tectonophysics 48, 77–106.

Panozzo, R.H., 1983. Two-dimensional analysis of shape-fabric using projections of digitized lines in a plane. Tectonophysics 95, 279–294.

Panozzo, R.H., 1984. Two-dimensional strain from the orientation of lines in a plane. Journal of Structural Geology 6, 215–221.

Passchier, C.W., Trouw, R.A.J., 1996. Microtectonics. Springer-Verlag, Berlin.

Patočka, F., Valenta, J., 1990. Geochemistry of metatrachytes and metarhyolites of the southern part of the Devonian Vrbno Group in the Horní Město area and tectonic setting of the origin of the metavolcanic protholith. Časopis pro mineralogii a geologii 35, 41–64 (in Czech).

Poirier, J.P., Guillopé, M., 1979. Deformation induced recrystallization of minerals. Bulletin de Minéralogie 102, 67–74.

Pouba, Z., 1962. Vysvětlivky k prehledné geologické mapě ČSSR 1:200,000, list M-33-XVIII, Jeseník (Legend of the geological map 1:200,000, Jeseník). ČSAV, Prague.

Price, N.J., Cosgrove, J.W., 1990. Analysis of Geological Structures. Cambridge University Press, Cambridge.

Ramberg, H., 1961. Relationship between concentric longitudinal strain and concentric shearing strain during folding of homogeneous sheets of rock. American Journal of Science 259, 382–390.

Ramberg, H., 1963. Fluid dynamics of viscous buckling applicable to folding of layered rocks. Bulletin of the American Association of Petrologists and Geologists 47, 484–505.

Ramberg, H., 1964. Selecting buckling of composite layers with contrasted rheological properties, a theory of simultaneous formation of several orders of folds. Tectonophysics 1, 307–341.

Ramsay, J.G., 1967. Folding and Fracturing of Rocks. McGraw-Hill, New York.

Ramsay, J.G., Huber, M., 1987. The Techniques of Modern Structural Geology. Volume 2: Folds and Fractures. Academic Press, London.

Rosenberg, C.L., Stünitz, H., 2003. Deformation and recrystallization of plagioclase along a temperature gradient: an example from the Bergell tonalite. Journal of Structural Geology 25, 389–408.

Roth, Z., 1962. Vysvětlivky k prehledné geologické mapě ČSSR 1:200,000, list M-33-XXIV, Olomouc (Legend of the geological map 1:200,000, Olomouc). ČSAV, Prague.

Rozkošný, I., Souček, J., 1989. Contribution to the petrology of the Žulová massif mantle. Acta Universitatis Carolinae, Geologica 2, 165–197.

Schulmann, K., Gayer, R., 2000. A model for an obliquely developed continental accretionary wedge developed by oblique collision: the NE Bohemian Massif. Journal of the Geological Society London 157, 401–416.

Schulmann, K., Mlčoch, B., Melka, R., 1996. High-temperature microstructures and rheology of deformed granite, Erzgebirge, Bohemian Massif. Journal of Structural Geology 18, 719–733.

Souček, J., 1978. Metamorphic zones of the Vrbno and Rejvíz Series, the Hrubý Jeseník Mts, Czechoslovakia. Tschermaks Mineralogische Petrographische Mitteilungen 25, 195–217.

Stabler, C.R., 1968. Simplified Fourier analysis of fold shapes. Tectonophysics 6, 343–350.

Štípská, P., Schulmann, K., Hoeck, V., 2000. Complex metamorphic zonation of the Thaya Dome; result of buckling and gravitational collapse of an imbricated nappe sequence. In: Cosgrove, J.W., Ameen, M.S. (Eds.), Forced Folds and Fractures Geological Society Special Publication, 169, pp. 197–211.

Štípská, P., Schulmann, K., Kröner, A., 2004. Vertical extrusion and middle crustal spreading of omphacite granulite: a model of syn-convergent exhumation (Bohemian Massif, Czech Republic). Journal of Metamorphic Geology 22, 179–198.

Stünitz, H., 1993. Transition from fracturing to viscous flow in a naturally deformed metagabbro. In: Boland, J.N., Fitz Gerald, J.D. (Eds.), Defects and Processes in the Solid State; Geoscience Applications; the McLaren Volume Developments in Petrology, 14. Elsevier, Amsterdam-New York, International, pp. 121–150.

Vernon, R.H., 1976. Metamorphic Processes. Murby, London; Wiley, New York.

Yund, R., Tullis, J., 1991. Compositional changes of minerals associated with dynamic recrystallization. Contributions to Mineralogy and Petrology 108, 346–355.